nature immunology

ARTICLES

https://doi.org/10.1038/s41590-022-01163-9

Check for updates

# Mechanisms of innate and adaptive immunity to the Pfizer-BioNTech BNT162b2 vaccine

Chunfeng Li[1], Audrey Lee[1], Lilit Grigoryan[1], Prabhu S. Arunachalam[1], Madeleine K. D. Scott[1,2], Meera Trisal[1], Florian Wimmers[1], Mrinmoy Sanyal[3], Payton A. Weidenbacher[3], Yupeng Feng[1], Julia Z. Adamska[1], Erika Valore[1], Yanli Wang[1], Rohit Verma[1], Noah Reis[1], Diane Dunham[4], Ruth O'Hara[5], Helen Park[6], Wei Luo[7], Alexander D. Gitlin[8,9], Peter Kim[3,10], Purvesh Khatri[1,2], Kari C. Nadeau[4,11,12] and Bali Pulendran[1,9,13] ✉

**Despite the success of the BNT162b2 mRNA vaccine, the immunological mechanisms that underlie its efficacy are poorly understood. Here we analyzed the innate and adaptive responses to BNT162b2 in mice, and show that immunization stimulated potent antibody and antigen-specific T cell responses, as well as strikingly enhanced innate responses after secondary immunization, which was concurrent with enhanced serum interferon (IFN)-γ levels 1 d following secondary immunization. Notably, we found that natural killer cells and CD8$^+$ T cells in the draining lymph nodes are the major producers of this circulating IFN-γ. Analysis of knockout mice revealed that induction of antibody and T cell responses to BNT162b2 was not dependent on signaling via Toll-like receptors 2, 3, 4, 5 and 7 nor inflammasome activation, nor the necroptosis or pyroptosis cell death pathways. Rather, the CD8$^+$ T cell response induced by BNT162b2 was dependent on type I interferon-dependent MDA5 signaling. These results provide insights into the molecular mechanisms by which the BNT162b2 vaccine stimulates immune responses.**

The BNT162b2 mRNA vaccine developed by Pfizer and BioNTech is the first US Food and Drug Administration (FDA)-approved mRNA vaccine in history. The vaccine demonstrated 95% efficacy against symptomatic coronavirus disease 2019 (COVID-19) caused by severe acute respiratory syndrome coronavirus 2 (SARS-CoV-2) infection in a phase-III trial[1,2]. However, despite its widespread use, the mechanisms by which BNT162b2 stimulates protective immunity remain largely unknown. BNT162b2 comprises *N*[1]-methyl-pseudouridine (m1Ψ) nucleoside-modified mRNA encapsulated in a lipid nanoparticle (LNP). Following administration in muscle, the mRNA is translated, resulting in the expression of the spike protein and spike-specific B and T cell responses[3]. Kariko et al. found that the m1Ψ-modification on RNA dampens the inflammatory response mediated by TLR3, TLR7 or RIG-I, and increases translational efficiency and biological stability[3,4]. mRNA vaccines encapsulated in LNPs were also found to induce a high magnitude of germinal center B (GC B) cell and follicular helper T cells ($T_{FH}$) responses after a single immunization[5–8].

Several studies have analyzed immune responses to the BNT162b2 vaccine in humans and revealed insights about the nature of the antibody and T cell responses to vaccination[1,2,9–13]. Despite our emerging understanding of immune responses to BNT162b2, there are major knowledge gaps on its mechanisms of action. For example, there is a paucity of understanding on the nature of the innate response to BNT162b2 and, in particular, how BNT162b2 is sensed by the host's innate immune system. Studies of mRNA vaccines against cancer demonstrate that they can trigger TLR4 (ref. [14]), TLR7 (ref. [15]) or STING[16] signaling pathways, but such knowledge is lacking in the context of BNT162b2. Arunachalam et al. used a systems vaccinology approach to analyze the innate and adaptive immune responses to vaccination with BNT162b2 in humans[9]. Our analysis demonstrated detectable neutralization antibody titers after primary immunization, which was enhanced considerably upon secondary immunization. Furthermore, there was only a modest innate immune response, at 1 or 7 d after primary immunization. Surprisingly however, secondary immunization with BNT162b2 induced a much higher magnitude of innate immune response than after primary vaccination[9]. This enhanced 'secondary innate response' was characterized by increased levels of IFN-γ in the plasma, enhanced transcriptional signatures of innate immunity and antiviral immunity in myeloid cells. However, the cellular sources of the rapidly produced IFN-γ and its role in the enhanced innate immune response after secondary vaccination remains unclear. Furthermore, although vaccination with BNT162b2 has been shown to induce substantial frequencies of antigen-specific CD8$^+$ T cell responses in the blood[9,17], there are currently no data on the nature of immune responses in tissues, as most studies have focused on analyzing immune responses in the blood. In addition, the in vivo distribution of the mRNA and the spike protein that it encodes, after intramuscular vaccination, remains poorly

[1]Institute for Immunity, Transplantation and Infection, Stanford University, Stanford, CA, USA. [2]Center for Biomedical Informatics, Department of Medicine, Stanford University School of Medicine, Stanford, CA, USA. [3]Department of Biochemistry & Stanford, ChEM-H, Stanford University, Stanford, CA, USA. [4]Sean N. Parker Center for Allergy & Asthma Research, Stanford, CA, USA. [5]Department of Psychiatry and Behavioral Sciences, Stanford University School of Medicine, Palo Alto, CA, USA. [6]Veterans Affairs Palo Alto Health Care System, Palo Alto, CA, USA. [7]Department of Microbiology and Immunology, Indiana University School of Medicine, Indianapolis, IN, USA. [8]Department of Physiological Chemistry, Genentech, South San Francisco, CA, USA. [9]Department of Pathology, Stanford University School of Medicine, Stanford, CA, USA. [10]Chan Zuckerberg Biohub, San Francisco, CA, USA. [11]Howard Hughes Medical Institute, Stanford University, Stanford, CA, USA. [12]Department of Medicine, Division of Pulmonary, Allergy and Critical Care Medicine, Stanford, CA, USA. [13]Department of Microbiology and Immunology, Stanford University School of Medicine, Stanford, CA, USA. ✉e-mail: bpulend@stanford.edu

understood. To address these knowledge gaps, we performed a detailed analysis of innate and adaptive immune responses to BNT162b2 vaccination in mice. In particular, we analyzed (1) the adaptive immune response induced by BNT162b2 after both primary and booster vaccines in organs including the lung and spleen; (2) the innate immune response in draining lymph nodes (dLNs), non-draining lymph nodes and other organs at the single-cell level, using systems immunology approaches; and (3) the innate sensing mechanisms that regulate antigen-specific antibody and T cell responses to BNT162b2 vaccination.

## Results

**BNT162b2 immunization stimulates robust germinal center responses.** To evaluate immune responses to BNT162b2, we immunized C57BL/6 mice on days 0 and 21 with 5 µg BNT162b2 by intramuscular injection (Fig. 1a). Anti-spike binding IgG responses, comprising both IgG1 and IgG2c, increased significantly at 14 d after primary immunization and persisted until day 21, while the secondary immunization increased the response more than tenfold (Fig. 1b). Consistent with binding antibody responses, neutralizing antibody responses against the SARS-CoV-2 wild-type (WT) strain and variants of concern including B1.1.7 (alpha), B.1.351 (beta), P.1 (gamma), B.1.617.2 (delta) and B.1.429 (epsilon) were detected on day 21 and increased significantly following secondary immunization (Fig. 1c). While the neutralizing titers against the alpha and epsilon variants did not differ significantly from those of the WT strain, neutralizing antibody titers at day 42 against the beta, gamma and delta variants were lower by 4.2-fold, 2.5-fold and 3.9-fold, respectively relative to the titers against the WT strain (Fig. 1c), consistent with findings in humans[18]. In addition to serological responses, we examined the responses of GC B cells ($CD19^+CD38^-CD95^+$) and $T_{FH}$ cells ($CD3^+CD4^+PD1^+CXCR5^+$) as well as plasma cells ($CD44^+CD138^+$). BNT162b2 immunization induced a strikingly high magnitude of GC B cells, $T_{FH}$ cells and plasma cells in dLNs, which peaked on day 7 and decreased by day 21 (Fig. 1d–f). Collectively, these data demonstrate the potent stimulation of humoral immune responses by BNT162b2. In addition, we tested antibody responses in mice immunized with 0.2 µg of the vaccine, which is an equivalent dose to that used in humans based on body weight[19,20]. The antibody kinetics mirrored the response induced by the higher dose, but the magnitude was approximately tenfold lower (Extended Data Fig. 1a).

**T cell response induced by BNT162b2 vaccination.** Next, we measured antigen-specific T cell responses in spleen and lung on days 21 and 42 after vaccination following the prime-boost immunization strategy presented in Fig. 1a. While the primary immunization elicited detectable antigen-specific $CD4^+$ and $CD8^+$ T cell responses in both tissues consistent with previous reports[8,21], there was a striking increase in the frequency of antigen-specific $CD8^+$ T cells after secondary immunization, especially in the lung, where we observed a median of 10% MHC-I tetramer-positive $CD8^+$ T cells on day 42 (Fig. 2a). There was a robust induction of spike-specific $CD8^+$ T cells secreting IFN-γ, tumor necrosis factor (TNF) and interleukin (IL)-2 following in vitro stimulation with an overlapping peptide pool (Fig. 2b). The $CD4^+$ T cell responses were primarily of the $T_H1$ type with little induction of IL-4 response (Fig. 2c), consistent with previous reports[8,21]. As tissue-resident memory T cells (TRMs) play an essential role in preventing local infection[22,23], we measured TRM ($CD3^+CD8^+CD44^+CD69^+CD103^+$) levels in the lung at day 21 and day 42 after BNT162b2 immunization and found that BNT162b2 immunization did not induce TRMs in the lung (Fig. 2d), consistent with previous findings[24]. The low dose (0.2 µg) of immunization resulted in ~fivefold lower magnitude of T cell responses (Extended Data Fig. 1b–d).

**BNT162b2 induces robust innate immune responses.** To profile the innate immune response induced by BNT162b2, we first analyzed the dLNs by multiparametric flow cytometry (Extended Data Fig. 2a). Frequencies of monocytes ($CD11b^+Ly6C^{hi}$), plasmacytoid DCs (pDCs; $CD11c^{lo}PDCA1^+$) and $CD103^+$ migratory DCs (mDCs) increased significantly on day 1 and returned to baseline levels on day 7 (Extended Data Fig. 2b). In contrast, resident DCs (rDCs; both $CD8a^+$ and $CD11b^+$) decreased in frequency on day 1 but increased significantly on day 7 (Extended Data Fig. 2b). Further, multiple innate immune cells including monocytes, macrophages ($CD11b^+Ly6C^{lo}F4/80^+$), pDCs and DC subsets ($CD8a^+$ rDCs, $CD11b^+$ rDCs, $CD103^+$mDCs and $CD11b^+$mDCs) were highly activated, as indicated by the enhanced expression of the activation marker CD86 (Fig. 3a). The low dose (0.2 µg) of immunization induced lower levels of innate cell activation (Extended Data Fig. 1e). These innate cell types remained activated until day 3 after immunization (Fig. 3b). In comparison, the innate cells were moderately activated in the contralateral lymph nodes (non-dLNs), lung and spleen (Fig. 3c,d).

Next, we analyzed serum cytokine responses using a Luminex assay. BNT162b2 immunization induced the release of many cytokines, including MCP1, MIP1b, IL-6 and CXCL10, as well as IFN-γ, that peaked at 6 h after immunization (Fig. 3e) in contrast to the significantly elevated levels of only two cytokines/chemokines (IFN-γ and CXCL10) in human volunteers after receiving the same vaccine[9]. It should, however, be noted that in the study in humans, Arunachalam et al. only measured plasma cytokine levels at 1 and 7 d after vaccination, and not at the earlier time point of 6 h examined in the current mouse study[9]. All the cytokines, except IFN-γ, returned to normal levels at day 3 after immunization. Strikingly, there was a significant induction of IFN-α (IFN-α2 and IFN-α4) in mice at 6 h, which was not observed in humans at the 1-d time point we examined[9]. Of note, the lower dose (0.2 µg) of immunization did not induce IFN-α as seen in humans; however, there was also an absence of IFN-γ response (Extended Data Fig. 1f), suggesting that there was not a human equivalent dose of BNT162b2 in mice.

**Single-cell transcriptomics of innate immunity to BNT162b2.** To further understand the cellular and molecular mechanisms involved in the immunogenicity of BNT162b2, we performed single-cell transcriptional profiling of cells in the dLNs 1, 3 and 7 d after immunization (Fig. 4a). As a benchmark, we compared the responses to BNT162b2 with those of the live attenuated yellow fever vaccine YF-17D, one of the most effective vaccines ever developed in humans[25]. Our previous work showed that YF-17D activates multiple subsets of DCs via several different Toll-like receptors (TLRs) to stimulate potent adaptive immune responses[26,27]. We used an 'enrich-mix' strategy in which $CD11b^+$ myeloid cells, pDCs ($CD11b^-CD11c^{lo}PDCA\text{-}1^+$) and DCs ($CD11c^+MHC\text{-}II^+$) were enriched by cell sorting and then mixed with total cell suspension at a ratio of 1:1 (Fig. 4a). The resulting cell suspension was subjected to droplet-based single-cell gene expression profiling. After quality control, we obtained 52,788 high-quality transcriptomes (Fig. 4b). Using dimensionality reduction via uniform manifold approximation and projection (UMAP) and graph-based clustering, we identified 20 cell clusters containing all major innate and adaptive immune cell types (Fig. 4b and Extended Data Fig. 3a). First, we analyzed the number of differentially expressed genes (DEGs) within each cluster. The YF-17D vaccine stimulated a profound DEG response in multiple cell types, as seen in previous study[28], which peaked at day 1 and returned to baseline by day 7. Interestingly, the mRNA vaccine stimulated a larger number of DEGs, especially in monocyte/macrophage, DCs and natural killer (NK) cells on day 1 that persisted until day 7 (Fig. 4c). Gene-set enrichment analysis using blood transcriptional modules (BTMs) revealed activation of type I interferon and antiviral responses in multiple cell types, which

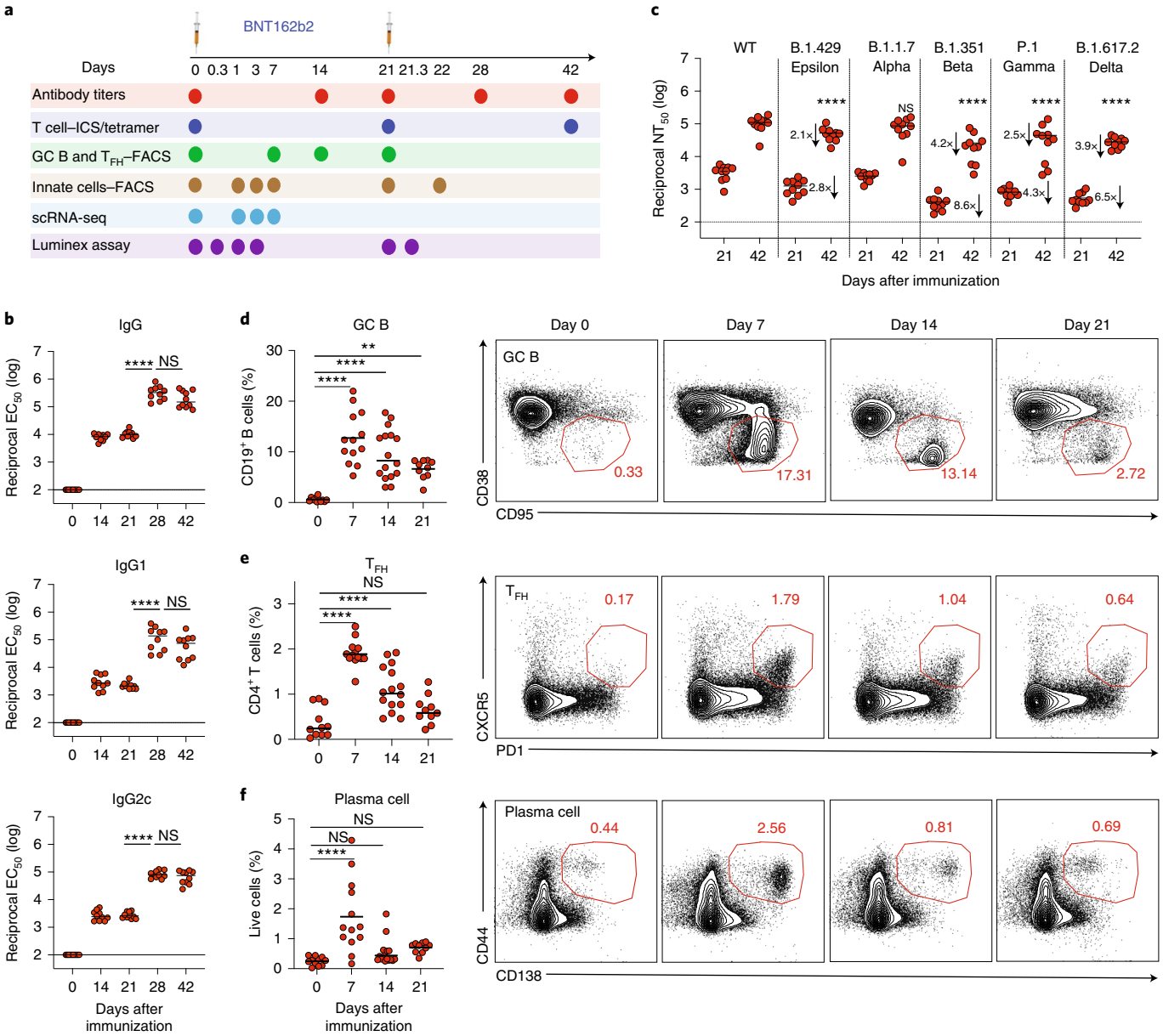


**Fig. 1 | BNT162b2 vaccine induces robust germinal center B cell and $T_{FH}$ cell response in mice. a**, Experimental timeline and tests. FACS, fluorescence-activated cell sorting; ICS, intracellular cytokine staining. **b**, Serum anti-spike IgG, IgG1a and IgG2c binding titers ($EC_{50}$) detected by ELISA. **c**, Pseudotyped lentivirus neutralization antibody titers ($NT_{50}$) against SARS-CoV-2 WT and variants of concern (B.1.429, B.1.1.7, B.1.351, P.1 and B.1.617.2) measured at days 21 and 42. $n=10$ mice per time point in **b** and **c**. **d**–**f**, GC B cell (**d**), $T_{FH}$ cell (**e**) and plasma cell (**f**) responses after BNT162b2 immunization. $n=11$, 13, 16 and 10 for days 0, 7, 14 and 21, respectively. Data were combined from two or more independent experiments. One-way analysis of variance (ANOVA) followed by Tukey's test was applied in **b**–**f**. $^{*}P<0.05$, $^{**}P<0.01$, $^{***}P<0.001$, $^{****}P<0.0001$. Differences between groups were considered significant for $P$ values < 0.05. NS, not significant.

peaked at day 1 and returned to baseline levels by day 7 (Fig. 4d). In contrast, cell cycle-associated genes and transcription-associated genes increased at day 1 and persisted to day 7, especially in NK cells and T cells (Fig. 4d). The overall responses were comparable to those of the YF-17D immunization (Extended Data Fig. 3b,c).

Arunachalam et al. demonstrated that the BNT162b2 vaccination in humans results in an enhanced innate immune response following the secondary vaccination in comparison with the primary vaccination[9]. A crucial aspect of that study was the discovery of an innate cell cluster (C8) using single-cell transcriptional profiling that emerged 1 d after secondary vaccination, a ~100-fold increase in comparison to the first day after primary vaccination. We determined that these cells were a transcriptional counterpart of an epigenetically programmed monocyte population that Wimmers et al. described in humans vaccinated with the H5N1 avian influenza subunit vaccine adjuvated with AS03 (H5N1 + AS03) (ref. [29]). The core transcriptional signature of these cells was an increased expression of interferon-stimulated genes (ISGs; *ISG15*, *GBP1*, *IFITM3*, *IFIH1*, *ANKRD22*, *IFI35*, *MX1*, *IRF1*, *IRF7*, *IRF8* and *STAT1*) and decreased expression of AP-1 transcription factors encoded by *FOS* and *JUN*[9,29]. Therefore, we asked if a similar cell population would also emerge in response to mRNA vaccination in mice. We re-embedded C2_mono_macrophage (a cluster containing a mix of monocyte and macrophage populations) and C15_macrophage

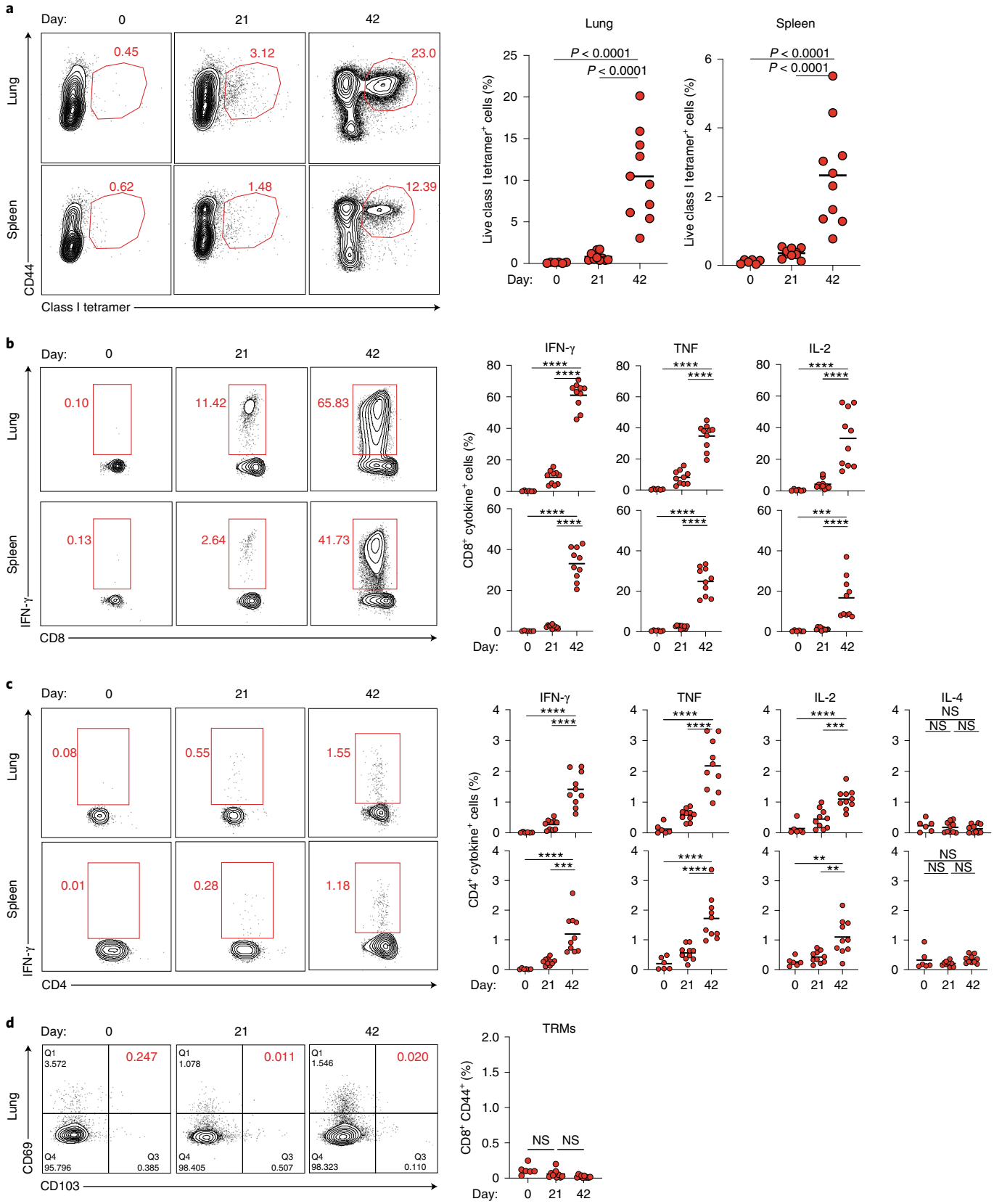


**Fig. 2 | T cell response induced by BNT162b2 vaccination in mice. a**, Class I tetramer-specific CD8⁺ T cell responses in lung and spleen at days 21 and 42 after BNT162b2 immunization. **b**,**c**, Antigen-specific CD8⁺ (**b**) and CD4⁺ (**c**) T cell responses in lung and spleen at days 21 and 42 as measured by ICS assay. **d**, TRMs in lung at days 21 and 42. Data were combined from two independent experiments. One-way ANOVA followed by Tukey's test was applied in **a**–**d**. $n = 6$ for day 0, and $n = 10$ for day 21 and day 42. $^{*}P < 0.05$, $^{**}P < 0.01$, $^{***}P < 0.001$, $^{****}P < 0.0001$.

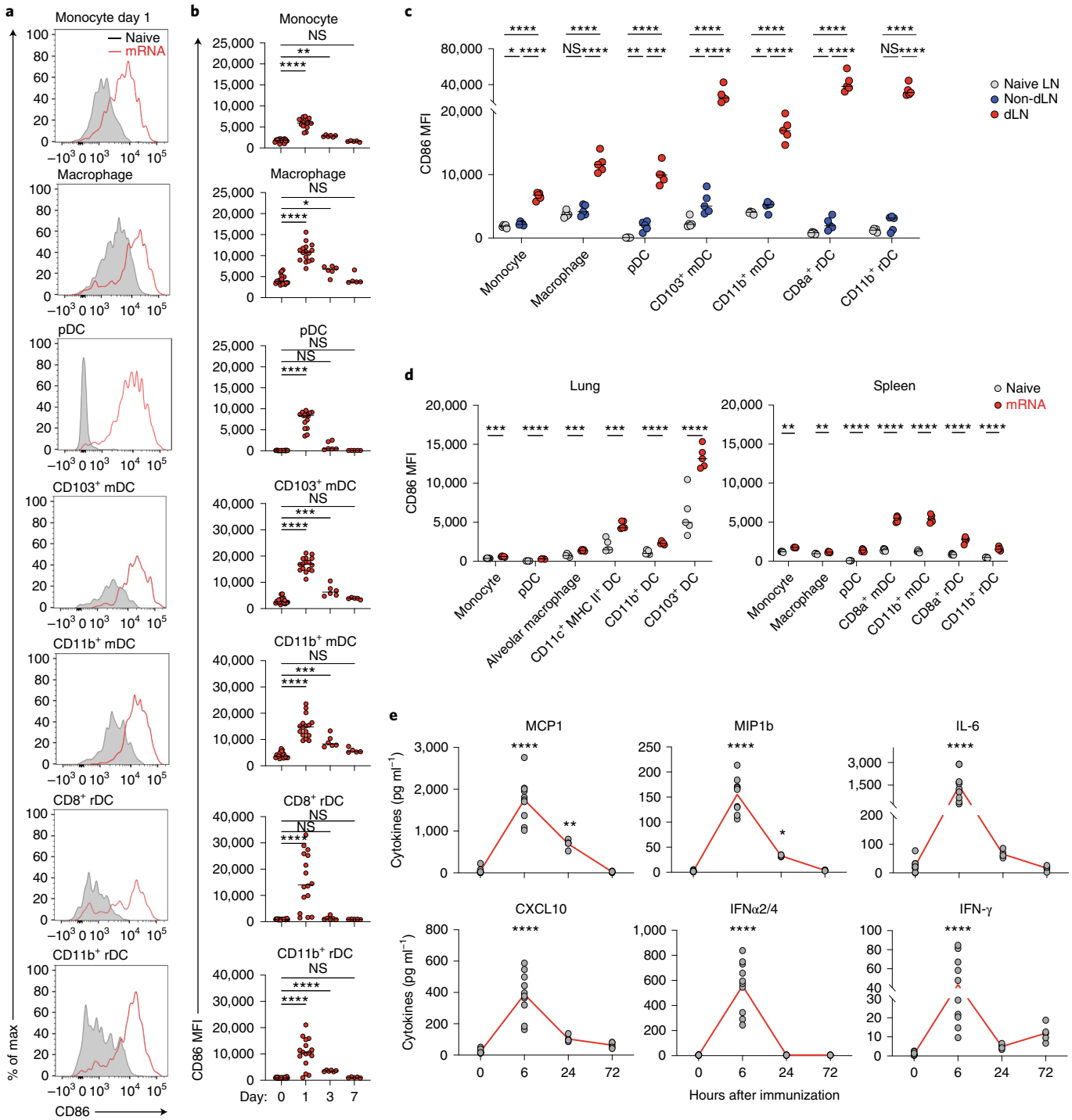


**Fig. 3 | BNT162b2 induces robust innate immune response in draining lymph nodes. a**, Activation of innate cells at day 1 after BNT162b2 immunization in dLNs indicated by activation marker CD86. **b**, Dynamics of innate cell activation at days 1, 3 and 7 after BNT162b2 immunization. $n = 20$, 16, 7 and 5 for days 0, 1, 3 and 7, respectively. **c**,**d**, Innate cell activation in contralateral lymph nodes (non-dLN) compared to that in dLNs (**c**), and in lung and spleen (**d**) at day 1 after prime. $n = 5$ for each group. **e**, Dynamics of cytokines in serum at 0, 6, 24 and 72 h after BNT162b2 immunization. $n = 10$ for 0 and 6 h; $n = 5$ for 24 h and 72 h. Data were combined from at least two independent experiments (**a**, **b** and **e**) or one representative of two independent experiments (**c** and **d**). One-way ANOVA followed by Tukey's test was applied in **b**–**e**. $^{*}P < 0.05$, $^{**}P < 0.01$, $^{***}P < 0.001$, $^{****}P < 0.0001$. MFI, mean fluorescence intensity.

clusters using genes that characterized the epigenetically remodeled monocyte population enriched in humans 21 d after vaccination with two doses of H5N1/AS03 (ref. [29]). Principal components were calculated from the 2,000 most variable genes within the cells originally part of macrophage clusters C2 and C15. Applying Louvain community detection to the nearest-neighbor graph structure derived from principal-component analysis embeddings with a resolution of 0.2, the monocytes/macrophages were segregated into 12 subclusters (Fig. 4e). Cluster membership differences between cells derived from mice treated with mRNA and YF-17D were mostly due to cells profiled on day 1 and day 3 (Fig. 4e). Strikingly, we found subclusters (3, 5, 7 and 8) that appeared within

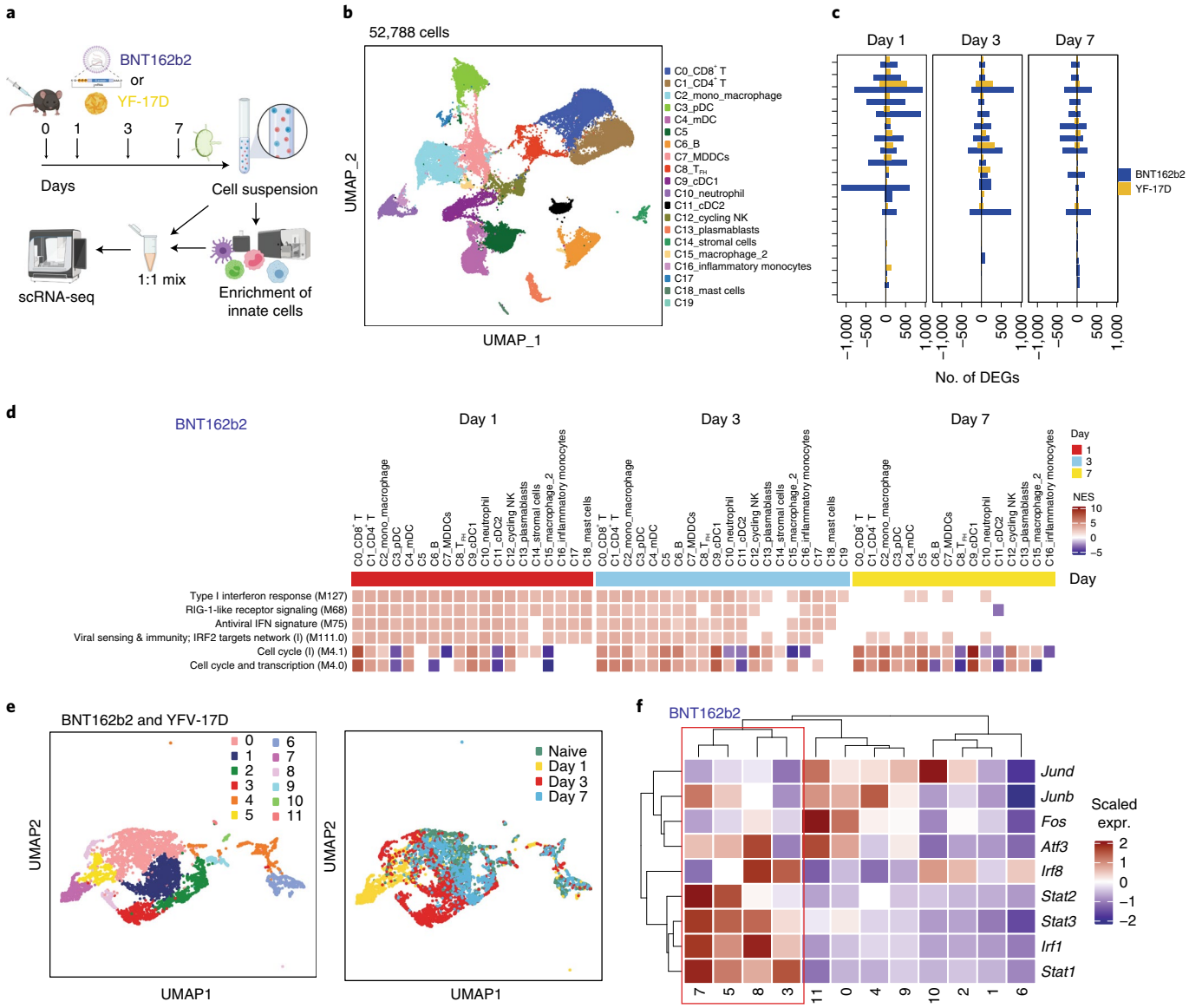


**Fig. 4 | Single-cell transcriptional response induced by BNT162b2 and YF-17D immunization in dLNs. a**, Experimental design and timeline. **b**, UMAP of cell types clustered by single-cell transcriptional analysis of 52,788 cells after quality control. MDDCs, monocyte-derived dendritic cells. **c**, DEGs induced by BNT162b2 and YF-17D immunization at days 1, 3 and 7. **d**, Significantly enriched interferon and cell cycle BTMs (false discovery rate < 0.05, absolute normalized enrichment score (NES) > 2) across all clusters from days 1 to 7 after BNT162b2 immunization. Only clusters with a significantly modulated pathway are shown. **e**, UMAP of subclusters in C2 (mono_macrophage) and C15 (macrophage) after BNT162b2 and YF-17D immunization, respectively. **f**, Heat map of key interferon response and AP-1 transcription factors after BNT162b2 immunization. Samples used for scRNA-seq were pooled from three independent experiments containing 8–10 mice.

1 and 3 d after immunization, with increased levels of *Irf8*, *Stat1*, *Stat2*, *Irf1* and *Stat3*, and decreased levels of *Atf3*, *Fos*, *Junb* and *Jund*, mirroring the innate immune cell populations described above (Fig. 4f and Extended Data Fig. 3d).

**BNT162b2 stimulates enhanced secondary innate immune response.** A hallmark of the immune response to BNT162b2 vaccination in humans is the striking increase in the innate immune response following secondary vaccination, relative to the response after primary vaccination[9]. To determine whether a similar effect was observed in mice, we measured serum cytokine/chemokine responses after the primary and secondary immunizations. Consistent with observations in humans[9], median IFN-γ response increased 8.6-fold, from 44.5 pg ml$^{-1}$ at 6 h after immunization (day 0.3) to 383.1 pg ml$^{-1}$ at 6 h after the secondary immunization (day 21.3; Fig. 5a). The data generated with the Luminex assay provided evidence that IFN-γ and other cytokines like IL-2, CCL2, CCL4 and CCL5 were enhanced at 6 h after the secondary immunization compared with those after the primary immunization, while there was no difference between prime and boost with a 0.2 μg dose (Extended Data Fig. 4a). Consistent with an increased IFN-γ level after secondary immunization, innate cells, including monocytes, macrophages and DCs, were more activated after secondary than after primary immunization, as judged by the level of CD86 expression (Fig. 5b).

In addition, we purified monocytes and quantified the expression of key ISGs and AP-1 transcription factors that distinguished cluster 8 from the other myeloid cells, defined in the human study

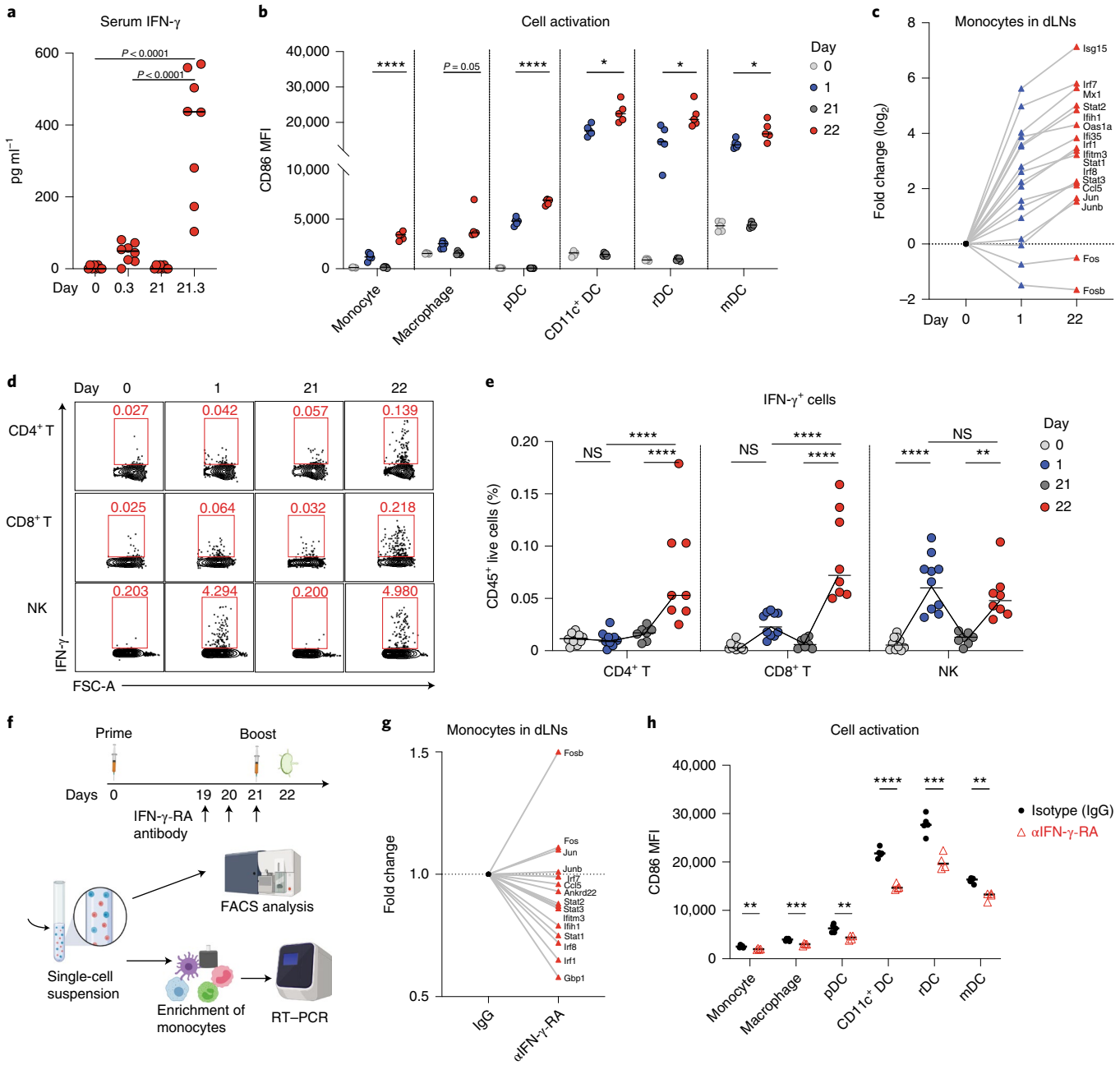


**Fig. 5 | Enhanced innate immune response after boost is mediated by IFN-γ production. a**, Serum IFN-γ measured by ELISA at days 0, 0.3 (6 h after prime), 21 and 21.3 (6 h after boost). $n = 8$ for each time point. **b**, Innate cell activation at days 0, 1, 21 and 22 after BNT162b2 immunization. $n = 5$. **c**, Fold change values of key interferon response genes and AP-1 transcription factors in monocytes at days 0, 1 and 22 after BNT162b2 immunization. **d**,**e**, Flow cytometry (**d**) and percentage (**e**) of cells producing IFN-γ in dLNs at the indicated times. $n = 10$ for days 0 and 1, and $n = 7$ and 8 for days 21 and 22, respectively. **f**, Experimental design and timeline. RT–PCR, PCR with reverse transcription. **g**, Fold change values of key interferon response genes and AP-1 transcription factors in IFN-γ-RA-neutralized group (αIFN-γ-RA) against isotype (IgG) control. **h**, Innate cell activation at day 22 after IFN-γ-RA neutralization. $n = 5$ for IgG group, $n = 4$ for αIFN-γ-RA-treated group. Data were combined from two independent experiments (**a** and **e**) or one representative of two independent experiments (**b**, **c**, **g** and **h**). One-way ANOVA followed by Tukey's test was applied in **a**. *P* values in **b** and **h** were determined using Student's *t*-tests (two-tailed). Two-way ANOVA followed by Tukey's test was applied in **e**. $^{*}P < 0.05$, $^{**}P < 0.01$, $^{***}P < 0.001$, $^{****}P < 0.0001$.

with BNT162b2 (ref. [9]). All the key ISGs (*Isg15*, *Mx1*, *Ifih1*, *Oas1a*, *Ifi35*, *Ifitm3*, *Ccl5*, *Irf1*, *Irf7*, *Irf8*, *Stat1*, *Stat2* and *Stat3*) were induced after the primary immunization, and importantly, the expression was increased further after the secondary immunization (Fig. 5c). Further, the AP-1 transcription factors encoded by *Fos* and *Fosb* were downregulated (Fig. 5c), as in previous studies[9,29]. Next, to identify the cellular origin of plasma IFN-γ, we performed ex vivo flow cytometry (Extended Data Fig. 4b). Notably, while the NK cells produced IFN-γ after both primary and secondary immunizations, CD4+ and CD8+ T cells contained the highest frequency of IFN-γ-expressing cells on day 22 (Fig. 5d,e). To determine whether the IFN-γ produced by T cells and NK cells within 1 d of secondary

immunization acted on myeloid cells to induce the expression of ISGs, we blocked the activity of IFN-γ in vivo with an IFN-γ receptor neutralizing antibody against the IFN-γ receptor, before secondary immunization on day 21 (Fig. 5f), and measured gene expression on day 22. We observed a significant reduction in the expression of all ISGs (*Gbp1*, *Ifih1*, *Ifitm3*, *Ankrd22*, *Ccl5*, *Irf1*, *Irf7*, *Irf8*, *Stat1*, *Stat2* and *Stat3*) in monocytes of anti-IFN-γ receptor antibody-treated mice versus mice treated with an isotype control (IgG), while the AP-1 transcription factors encoded by *Fos*, *Fosb*, *Jun* and *Junb* were upregulated (Fig. 5g). Furthermore, activation of monocytes, macrophages and DCs was significantly reduced in IFN-γ-receptor antibody-treated mice (Fig. 5h), suggesting that IFN-γ signaling plays an important role in the innate immune activation induced by BNT162b2. We also measured spike-specific T cell and antibody responses on day 42 after IFN-γ receptor blockade. We found that the antigen-specific CD4$^+$ and CD8$^+$ T cell responses did not differ significantly in the lung, nor was there a difference in antibody response (Extended Data Fig. 4c–e). However, there was a ~twofold reduction in the spike-specific CD8$^+$ T cells producing IFN-γ in the spleen (Extended Data Fig. 4c). To further delineate the relative importance of T cells versus NK cells in producing the burst of IFN-γ on day 22, we depleted NK or T cells (CD4$^+$ and CD8$^+$ T cells) before boost using NK1.1 or CD4/CD8-depletion antibodies. The T cell depletion, but not NK cell depletion, abrogated serum IFN-γ on day 22 (Extended Data Fig. 4f), 1 d after the boost demonstrating that the CD4$^+$ and CD8$^+$ T cells were the primary source of the circulating IFN-γ. Consistent with this, the activation of innate immune cells measured by mean fluorescence intensity of CD86 expression was more substantially reduced in T cell-depleted mice than in the control mice or mice depleted of NK cells (Extended Data Fig. 4g).

**mRNA uptake by lymph node dendritic cells and macrophages.** Many characteristics of LNP-mRNA vaccines, including size of the LNP, $pK_a$ of the ionizable lipid, and lipid gradients, affect the tissue and cell specificity of the mRNA vaccine[15,30]. Using single-cell RNA-sequencing (scRNA-seq) data, we investigated the cells containing spike mRNA in the dLNs. We observed high levels of spike mRNA reads on day 1 that decreased sharply by day 3 (Fig. 6a). The reads were primarily restricted to clusters 2 and 4, which represent monocyte/macrophages and mDCs, respectively (Fig. 6a). Quantification of cells with at least one read per cell demonstrated that 40% of monocyte/macrophages and 20% of mDCs contained spike mRNA on day 1 (Fig. 6b). The frequency of these cells increased after vaccination (Fig. 6c). We also measured mRNA in various tissues using real-time PCR and found that the dLNs contained the highest concentration of mRNA (Fig. 6d). Interestingly, the spleen tissue also contained mRNA but at a much lower concentration (Fig. 6d). Consistent with the transcriptional data, serum concentration of spike protein increased on day 1 and decreased by day 7 (Fig. 6e). There was a small amount of mRNA in other tissues such as muscle, liver, lung and non-dLNs (Fig. 6e), consistent with previous reports[31]. Finally, we analyzed the gene expression profile associated with the spike mRNA signals in macrophages and mDCs (Fig. 6f). In both cell clusters, the spike mRNA signal was associated strongly with interferon-related and innate immune response-related BTMs including type I interferon response (M127), activated DCs (M64 and M67) in C2, chemokine cluster (II; M27.1), TLR and inflammatory signaling (M16) in C4, and RIG-I-like receptor signaling (M68) and antiviral IFN signature (M75) in both C2 and C4 (Fig. 6f), suggesting direct activation of innate immune signaling by the mRNA. Notably, *Ifih1*, the gene encoding MDA5, and downstream targets of MDA5 signaling were highly correlated with the spike mRNA signal in monocytes and macrophages (Fig. 6g). On the other hand, expression of TLRs and MyD88 was highly associated with the spike mRNA levels in the mDCs (Fig. 6g).

**BNT162b2 stimulates CD8$^+$ T cell responses via MDA5–IFN-α axis.** TLRs are the most studied sensors of pathogen-associated molecular patterns[32]. TLR3 and TLR7 recognize double-stranded and single-stranded RNA, respectively[33–35]. Therefore, we first examined whether deficiency of these receptors results in a diminished immune response to BNT162b2. However, immunization of *Tlr3*$^{-/-}$ or *Tlr7*$^{-/-}$ mice did not cause a reduction of antibody or T cell responses (Extended Data Fig. 5a–c), suggesting that they are not the primary sensors of BNT162b2 in vivo. Previous evidence indicates that the SARS-CoV-2 spike protein binds to and stimulates TLR2 and TLR4 signaling[36,37]. Further, we have shown that the immune responses to the seasonal flu and other unadjuvanted vaccines are controlled by microbiota via the TLR5 pathway[38]. Therefore, in addition to examining TLR3 and TLR7, we measured antibody and T cell responses in *Tlr2*$^{-/-}$, *Tlr4*$^{-/-}$ and *Tlr5*$^{-/-}$ mice. None of the mice demonstrated an impaired immune response to BNT162b2 vaccination (Extended Data Fig. 5d–i), providing evidence that these receptors are also not the primary sensors of BNT162b2.

Inflammasomes are critical regulators of innate immunity that regulate adaptive immunity to vaccines and adjuvants[39,40]. We examined the role of the inflammasome pathway using *Asc*$^{-/-}$ (also known as *Pycard*$^{-/-}$) and *Nlrp3*$^{-/-}$ mice and found no significant difference in antibody or T cell responses in comparison to WT mice (Extended Data Fig. 6a–c). Next, we examined the role of the cGAS–STING pathway, a cytoplasmic nucleic acid-sensing mechanism[41,42]. *Cgas*$^{-/-}$ and *Sting*$^{-/-}$ mice did not display a reduced response (Extended Data Fig. 7a–c), suggesting that these proteins do not play a role in immunogenicity of BTN162b2. Kim et al. reported that damage-associated molecular patterns, released during cell death pathways such as necroptosis, regulate immunity to adjuvants[43]. Like the adjuvant MF59 (ref. [43]), BNT162b2 induced damage-associated molecular pattern signals, including double-stranded DNA and HMGB1 peaking at 24 h after immunization, and uric acid peaking 2 d after immunization (Extended Data Fig. 8a–c). However, *Ripk3*$^{-/-}$ and *Gsdmd*$^{-/-}$ mice displayed no effect of BNT162b2-mediated T cell and antibody responses compared with littermate controls (Extended Data Fig. 8d–i).

The RIG-I-like receptor family of proteins sense cytosolic RNA and are a second family of putative sensors of BNT162b2[44,45]. To evaluate whether RIG-I-like receptors are involved in mRNA recognition, we immunized mice deficient in MDA5. There was no reduction in the antibody responses (Fig. 7a,b). Interestingly, *Mda5*$^{-/-}$ mice had a striking reduction in the frequency of antigen-specific CD8$^+$ T cells as evidenced by fewer class I tetramer-specific CD8$^+$ T cells and IFN-γ-producing CD8$^+$ T cells after primary (Extended Data Fig. 9) and secondary (Fig. 7c,d) immunizations, suggesting that the MDA5 sensing of BNT162b2 is responsible for the induction of spike-specific CD8$^+$ T cell responses. We also observed that the concentration of serum total IFN-α was below the detection limit in *Mda5*$^{-/-}$ mice, while the WT B6 mice produced as much as 2 ng ml$^{-1}$ of IFN-α at 6 h, as measured by ELISA (Fig. 7e). Further, the activation of innate immune cells measured by CD86 expression was significantly downregulated in these mice (Fig. 7f). As type I interferons are known to directly stimulate clonal expansion of CD8$^+$ T cells[46,47], we examined whether mice deficient in IFNAR1 are likewise deficient in CD8$^+$ T cell responses. Consistent with our hypothesis, there was a striking reduction in spike-specific CD8$^+$ T cell frequencies enumerated by tetramer staining in the lung and spleen of *Ifnar1*$^{-/-}$ mice (Fig. 7g). In addition, there was also a significant but incomplete downregulation in the frequency of spike-specific T cells secreting IFN-γ (Fig. 7h); however, there was only a negligible effect on the antibody response (Fig. 7i). Moreover, the serum cytokine/chemokine responses (Fig. 7j,k) and the activation of innate immune cells measured by CD86 expression were also reduced (Fig. 7l). Collectively, these data show that MDA5 senses BNT162b2 to induce expression of IFN-α, which stimulates

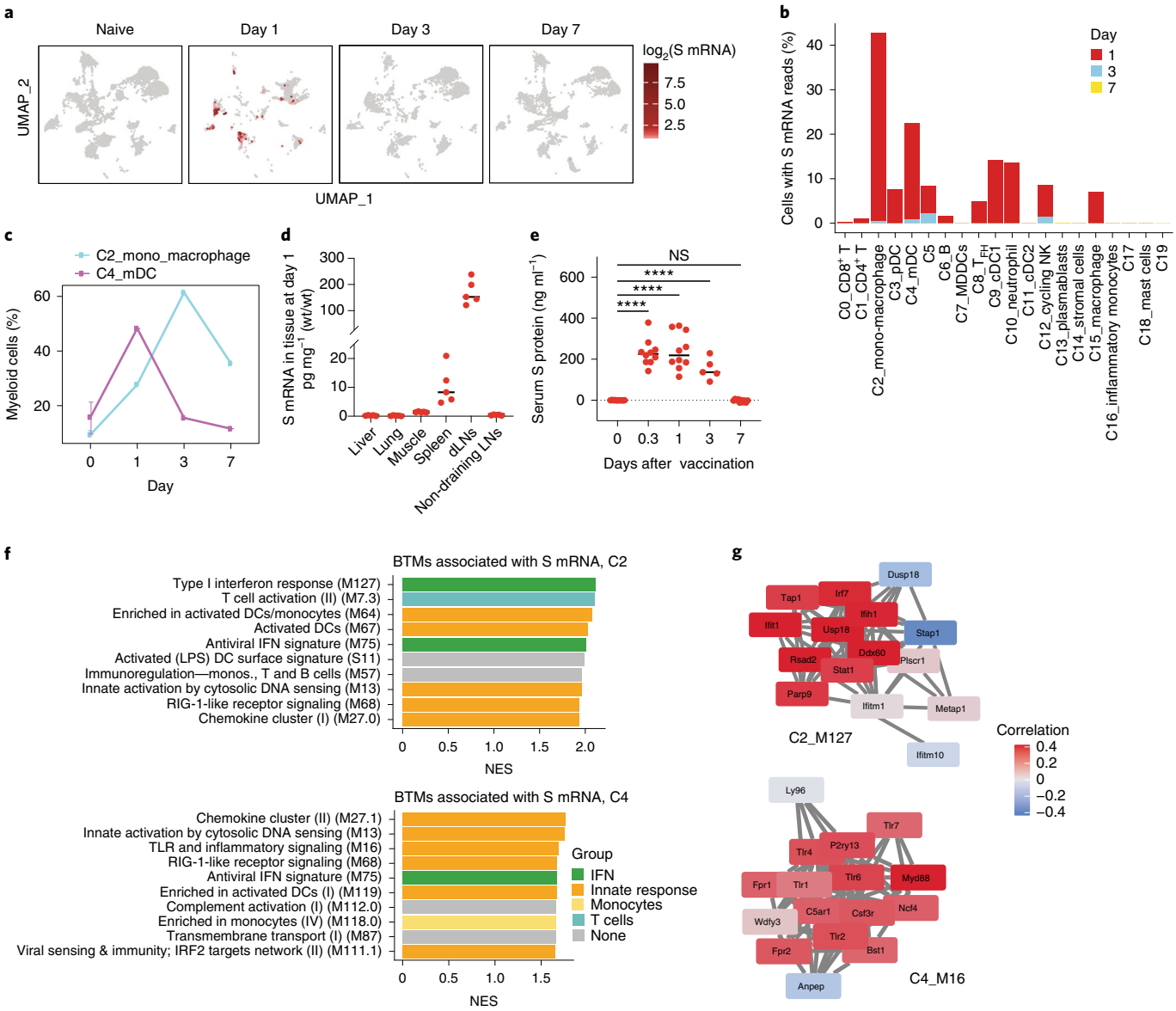


**Fig. 6 | Uptake of BNT162b2 by dendritic cells and macrophages in draining lymph nodes. a**, Distribution of spike mRNA at the single-cell level (read > 1 per cell) from days 1 to 7 after BNT162b2 immunization. Cell clusters of UMAP are as shown in Fig. 4b. **b**, The percentage of cells with spike mRNA reads in each cluster over time. **c**, The percentage of C2 and C4 in myeloid cells over time. **d**, Distribution of spike mRNA in tissues at day 1 after BNT162b2 immunization measured by TaqMan-based RT–PCR. $n = 5$ for each tissue. **e**, Spike protein in mouse serum detected by ELISA. $n = 5$ or 10. **f**, The BTMs associated with spike mRNA signal in C2_mono_macrophage and C4_mDCs. **g**, The correlation between spike mRNA signal and gene expression in BTM module M127 (type I interferon response) in C2_mono_macrophage and M16 (TLR and inflammatory signaling) in C4_mDCs, respectively. Samples used for scRNA-seq were pooled from three independent experiments containing 8–10 mice. Data were one representative of two independent experiments (**d**) or combined from two independent experiments (**e**). One-way ANOVA followed by Tukey's test was applied in **e**. $^{****}P < 0.0001$. LPS, lipopolysaccharide.

antigen-specific CD8$^+$ T cell expansion via IFNAR1, to promote a high magnitude of antigen-specific CD8$^+$ T cells. Thus, MDA5 deficiency leads to IFN-α deficiency, which in turn leads to reduced CD8$^+$ T cell response after primary vaccination, which then leads to reduced recall responses. Finally, we also detected a reduced frequency of CD8$^+$ T cells, and negligible reduction of IgG titers in *Batf3*$^{-/-}$ mice (Extended Data Fig. 10), which lack cross-presenting CD8α$^+$ DCs[48], suggesting the cross-presentation is important for BNT162b2-induced T cell responses.

## Discussion

The current study, involving a detailed analysis of immune responses to vaccination of mice with the BNT162b2 vaccine, provided several new mechanistic insights (Fig. 8). As is the case in humans, after secondary immunization of mice, BNT162b2 induced a tenfold greater magnitude of antigen-specific binding and neutralizing antibodies, and potent GC B cell and $T_{FH}$ responses. Surprisingly, there was a strikingly high magnitude of antigen-specific CD8$^+$ T cells in the lung and spleen, after the secondary immunization. The higher magnitude of T cell response in lung than in spleen is not unique to the mRNA vaccine, as we have observed this in mice immunized with YF-17D[49], and with AddaVax or MF59 plus Ova[43]. Experiments using a low dose (0.2 μg) of vaccine also resulted in similar B cell and T cell responses, but the magnitude was fivefold to tenfold lower than the high dose. Consistent with findings in humans[9], we observed in mice enhanced innate immune responses,

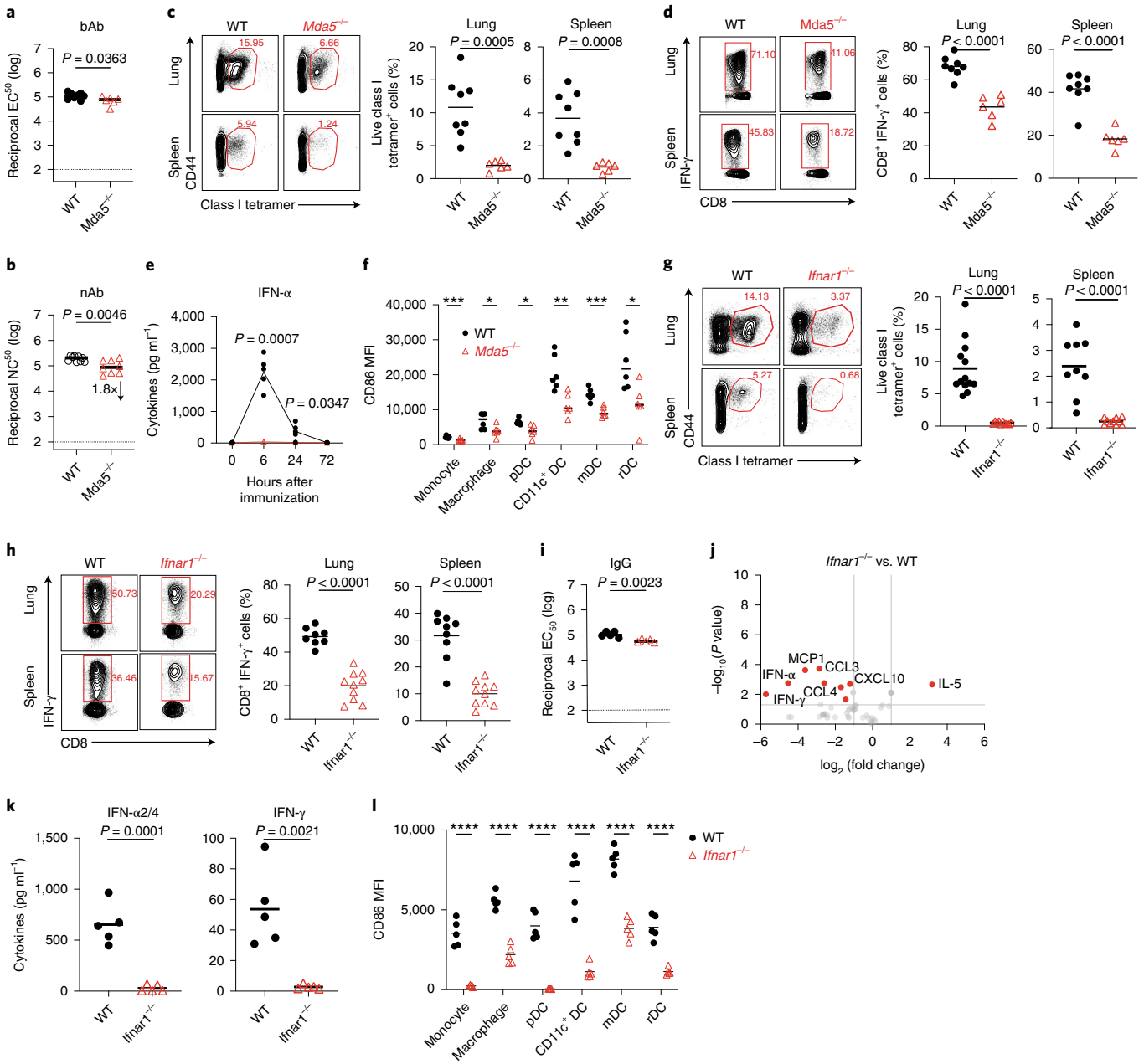


**Fig. 7 | MDA5–IFNAR1 axis is important for BNT162b2-induced CD8⁺ T cell response. a**,**b**, Binding antibody (bAb) (**a**) and neutralizing antibody (nAb) (**b**) titers of WT and *Mda5*$^{-/-}$ mice at day 42. In **a**, $n=8$ for WT, $n=6$ for *Mda5*$^{-/-}$. In **b**, $n=9$ for WT, $n=8$ for *Mda5*$^{-/-}$. **c**, Class I tetramer-specific CD8⁺ T cell response in the lung and spleen of WT and *Mda5*$^{-/-}$ mice measured at day 42 after BNT162b2 immunization as shown in Fig. 1a. **d**, Antigen-specific CD8⁺ T cell response in lung and spleen of WT and *Mda5*$^{-/-}$ mice detected at day 42 by ICS assay. In **c** and **d**, $n=8$ for WT, $n=6$ for *Mda5*$^{-/-}$. **e**, Serum total IFN-α levels in WT ($n=5$) and *Mda5*$^{-/-}$ ($n=4$) mice at 0, 6, 24 and 72 h measured by ELISA. **f**, Activation of innate cells in WT and *Mda5*$^{-/-}$ mice at day 1 after prime. $n=6$ for each group. **g**, Class I tetramer-specific CD8⁺ T cell response in lung and spleen tissue of WT and *Ifnar1*$^{-/-}$ mice measured at day 42. For lung, $n=13$ for WT, $n=10$ for *Ifnar1*$^{-/-}$; for spleen, $n=9$ for WT, $n=10$ for *Ifnar1*$^{-/-}$. **h**, Antigen-specific CD8⁺ T cell response in lung and spleen of WT and *Ifnar1*$^{-/-}$ mice detected at day 42 by ICS assay. For lung, $n=8$ for WT, $n=10$ for *Ifnar1*$^{-/-}$; for spleen, $n=9$ for WT, $n=10$ for *Ifnar1*$^{-/-}$. **i**, IgG titers of WT and *Ifnar1*$^{-/-}$ mice at day 42. $n=5$ for each group. **j**, Cytokines/chemokines in serum of WT and *Ifnar1*$^{-/-}$ mice at 6 h measured by Luminex. **k**, Serum IFN-α2/4 and IFN-γ levels in WT and *Ifnar1*$^{-/-}$ mice at 6 h. $n=5$ for each group. **l**, Activation of innate cells in WT and *Ifnar1*$^{-/-}$ mice at day 1 after prime. $n=5$ for each group. Data were combined from at least two independent experiments (**b**–**d** and **g** and **h**) or one representative experiment (**a**, **e**, **f** and **i**–**l**). *P* values were determined using Student's *t*-tests (two-tailed). $^{*}P<0.05$, $^{**}P<0.01$, $^{***}P<0.001$, $^{****}P<0.0001$.

including enhanced plasma IFN-γ concentrations, enhanced activation of DCs and myeloid cells in the dLNs, with a potent transcriptional signature of ISGs, and diminished expression of AP-1 transcription factor genes, after the secondary immunization with BNT162b2. We extended these findings to show that the CD4⁺ and CD8⁺ T cells were the primary source of serum IFN-γ 1 d after secondary immunization, which results in the enhanced myeloid cell activation after the secondary immunization. The heightened IFN-γ response following secondary immunization could conceivably enhance innate antiviral immunity during the first few days or weeks of vaccination, a period during which antigen-specific T cell and B cell responses are still nascent. In line with this notion,

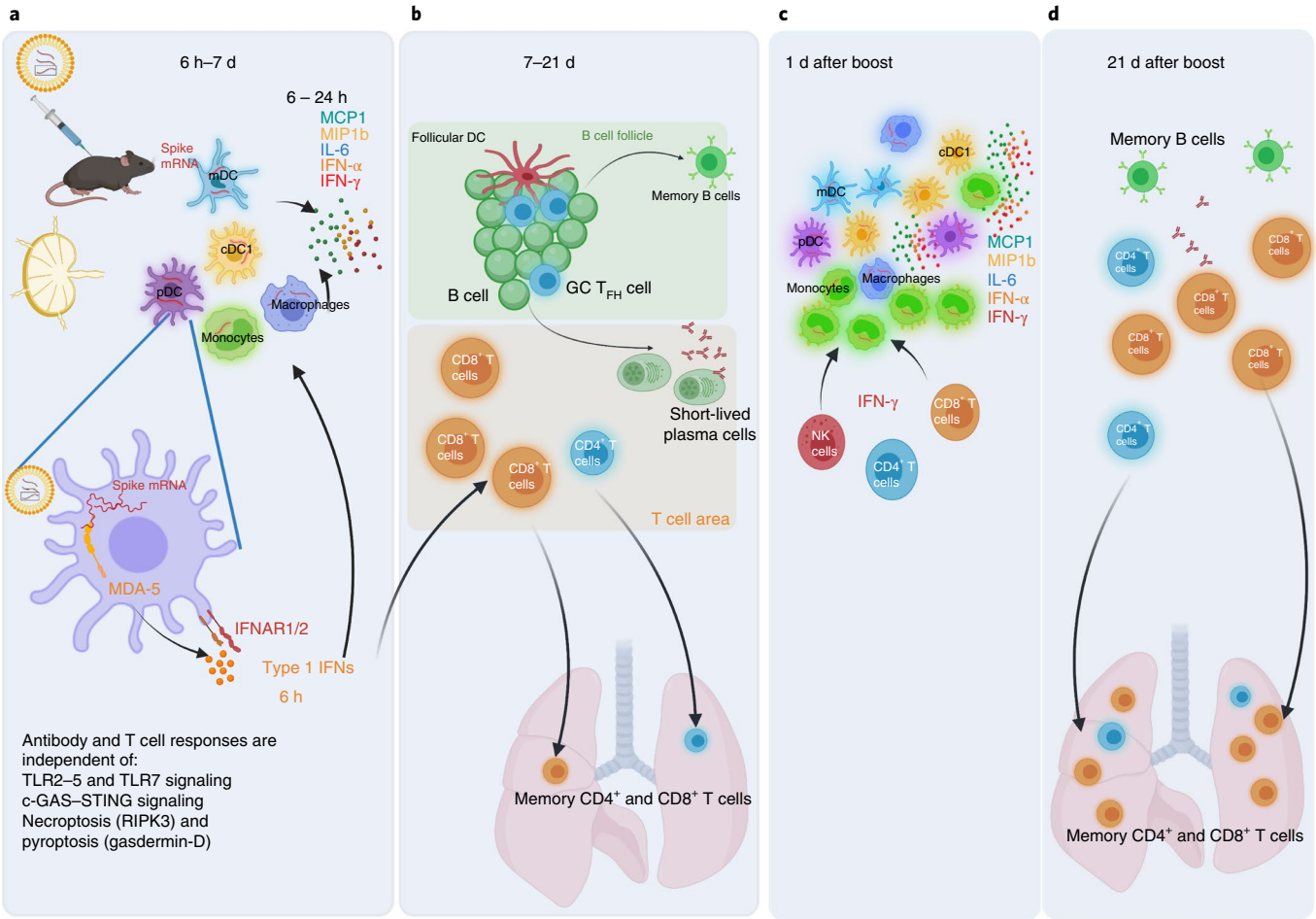


**Fig. 8 | Depicting the mode of action of BNT162b2 in vivo. a**. At 6 h to 7 d after BNT162b2 prime, DCs and macrophages in dLNs take up the vaccine and express spike proteins. These innate cells are highly activated and produce cytokines, including IL-6, IFN-α, IFN-γ, MCP1 and MIP1b. In this process, the MDA5–IFNAR1 signaling pathway is essential for IFN-α production and innate cell activation. **b**, At days 7 to 21, strong GC B and $T_{FH}$ cell responses are induced in B cell follicles. The CD8$^+$ T cell response is increased mildly in both spleen and lung tissue. **c**, At days 1 to 3 after boost, much more IFN-γ is produced by NK, CD4$^+$ and CD8$^+$ T cells, contributing to the enhanced innate cell activation after boost. **d**, At 21 d after boost, the antibody response, CD4$^+$ and CD8$^+$ T cell responses increase significantly. The MDA5–IFNAR1 signaling pathway is essential for CD8$^+$ T cell responses in both spleen and lung tissue.

Wimmers et al. showed that vaccination with H5N1 + AS03 induces epigenetic changes in monocytes and myeloid DCs associated with enhanced IRF accessibility and heightened resistance to infection with unrelated blood-borne viruses, such as dengue virus and Zika virus[29]. Whether BNT162b2 can also cause the epigenetic changes on a genomic level to provide broader protection against other infectious diseases remains an open question in both humans and mice.

The distribution and dynamics of the BNT162b2 mRNA and the spike protein encoded by it, in tissues and cell types in vivo remains unclear. In this study, we found that BNT162b2 mRNA could be detected in mDCs and monocyte/macrophage subsets in the dLNs for at least 7 d following intramuscular immunization. Furthermore, mRNA could be detected in the spleen, and the spike protein itself was detectable in the serum, for up to 7 d after immunization.

Another insight to emerge from this study is how the innate immune system senses the BNT162b2 mRNA vaccine and modulates adaptive immunity. By analyzing responses in various strains of knockout mice, we found that induction of antigen-specific T cell and antibody responses was independent of TLR2–TLR5 and TLR7, or the STING–cGAS DNA-sensing pathway, and independent of NLRP3-dependent ASC inflammasome activation. Furthermore, mice deficient in RIP3 kinase and gasdermin D, the central mediators of necroptosis[50,51] and pyroptosis[52] respectively, mounted normal T and antibody responses to BNT162b2, arguing that these cell death pathways were not essential for the immunogenicity of this vaccine. However, we found that the MDA5–IFNAR1 signaling pathway is critical for the CD8$^+$ T cell response induced by BNT162b2. A previous study showed that MDA5 deficiency resulted in a modest impairment of antigen-specific CD8$^+$ T cell response following primary immunization with OVA+polyI:C, but a more pronounced impairment of secondary T cell responses[53]. MDA5 deficiency affects clonal expansion of CD8$^+$ T cells after primary as well as secondary immunization with BNT162b2 via impaired production of IFN-α, within the first few hours of primary vaccination. These data are consistent with studies showing a critical role for type I interferon responses in the clonal expansion of antigen-specific CD8$^+$ T cells[46]. mRNA is known to spontaneously form double-stranded RNA structures, and it is likely that MDA5 recognizes these double-stranded elements[54] in the target cells.

Whether these findings with BNT162b2 are applicable to other mRNA vaccines, such as mRNA-1273 from Moderna[55] and MRT5500 from Sanofi[56], remains to be determined. Although our data provide no evidence for a role for TLR2–TLR5 and TLR7, Alameh et al.

showed that GC B cell and $T_{FH}$ cell responses induced by a different mRNA vaccine (a nucleoside-modified HA mRNA-LNP vaccine) is dependent on MyD88 but not MAVS[57]. Whether this difference is due to synergistic triggering through multiple TLRs, or differences between the BNT162b2 vaccine from Pfizer-BioNTech versus the vaccine used by Alameh et al. remains to be determined.

As will be appreciated, the aforementioned experiments in mice have revealed several new mechanistic insights about the innate and antigen-specific T and B cell responses induced by the BNT162b2 mRNA vaccine. A key question relates to the relevance of these various responses to protection against infection and disease caused by SARS-CoV-2. Israelow et al. found that mRNA-mediated protection from SARS-CoV-2 infection in mouse models is primarily mediated by humoral responses, while the cell-mediated immune responses are efficient in clearing infection[24]. The extent of the immunological defects observed in the mice deficient in MDA5 and IFNAR1, as well as the defects in secondary innate immunity caused by blockade of IFN-γ activity before secondary vaccination, remains to be determined. Finally, it should be remembered that, while the immune systems of mice and humans are broadly similar, nearly 80 million years of evolutionary divergence of these species have resulted in many differences in the details of how their immune systems work[58]. Therefore, the results obtained in mice should be interpreted in the context of similar studies in humans, in order to arrive at an integrated understanding of how our immune systems sense and respond to mRNA vaccines[58–60]. In summary, our study provides rich insights into the mechanism of BNT162b2's effects in vivo. These results not only help us better understand the mechanism of the BNT162b2 vaccine but also will help in the design of improved vaccines in the future.

## Online content

Any methods, additional references, Nature Research reporting summaries, source data, extended data, supplementary information, acknowledgements, peer review information; details of author contributions and competing interests; and statements of data and code availability are available at https://doi.org/10.1038/s41590-022-01163-9.

Received: 20 October 2021; Accepted: 17 February 2022;
Published online: 14 March 2022

## References

1. Polack, F. P. et al. Safety and efficacy of the BNT162b2 mRNA COVID-19 vaccine. *N. Engl. J. Med.* **383**, 2603–2615 (2020).
2. Walsh, E. E. et al. Safety and immunogenicity of two RNA-based COVID-19 vaccine candidates. *N. Engl. J. Med.* **383**, 2439–2450 (2020).
3. Kariko, K. et al. Incorporation of pseudouridine into mRNA yields superior nonimmunogenic vector with increased translational capacity and biological stability. *Mol. Ther.* **16**, 1833–1840 (2008).
4. Kariko, K., Buckstein, M., Ni, H. & Weissman, D. Suppression of RNA recognition by Toll-like receptors: the impact of nucleoside modification and the evolutionary origin of RNA. *Immunity* **23**, 165–175 (2005).
5. Turner, J. S. et al. SARS-CoV-2 mRNA vaccines induce persistent human germinal centre responses. *Nature* **596**, 109–113 (2021).
6. Lederer, K. et al. SARS-CoV-2 mRNA vaccines foster potent antigen-specific germinal center responses associated with neutralizing antibody generation. *Immunity* **53**, 1281–1295 e1285 (2020).
7. Pardi, N. et al. Nucleoside-modified mRNA vaccines induce potent T follicular helper and germinal center B cell responses. *J. Exp. Med.* **215**, 1571–1588 (2018).
8. Laczko, D. et al. A single immunization with nucleoside-modified mRNA vaccines elicits strong cellular and humoral immune responses against SARS-CoV-2 in mice. *Immunity* **53**, 724–732 (2020).
9. Arunachalam, P. S. et al. Systems vaccinology of the BNT162b2 mRNA vaccine in humans. *Nature* **596**, 410–416 (2021).
10. Tarke, A. et al. Impact of SARS-CoV-2 variants on the total $CD4^+$ and $CD8^+$ T cell reactivity in infected or vaccinated individuals. *Cell Rep. Med.* **2**, 100355 (2021).
11. Sahin, U. et al. BNT162b2 vaccine induces neutralizing antibodies and poly-specific T cells in humans. *Nature* **595**, 572–577 (2021).
12. Liu, J. et al. BNT162b2-elicited neutralization of B.1.617 and other SARS-CoV-2 variants. *Nature* **596**, 273–275 (2021).
13. Painter, M. M. et al. Rapid induction of antigen-specific $CD4^+$ T cells is associated with coordinated humoral and cellular immunity to SARS-CoV-2 mRNA vaccination. *Immunity* **54**, 2133–2142 (2021).
14. Zhang, H. et al. Delivery of mRNA vaccine with a lipid-like material potentiates antitumor efficacy through Toll-like receptor 4 signaling. *Proc. Natl Acad. Sci. USA* **118**, e2005191118 (2021).
15. Kranz, L. M. et al. Systemic RNA delivery to dendritic cells exploits antiviral defence for cancer immunotherapy. *Nature* **534**, 396–401 (2016).
16. Miao, L. et al. Delivery of mRNA vaccines with heterocyclic lipids increases anti-tumor efficacy by STING-mediated immune cell activation. *Nat. Biotechnol.* **37**, 1174–1185 (2019).
17. Sahin, U. et al. COVID-19 vaccine BNT162b1 elicits human antibody and $T_H1$ T cell responses. *Nature* **586**, 594–599 (2020).
18. Planas, D. et al. Reduced sensitivity of SARS-CoV-2 variant delta to antibody neutralization. *Nature* **596**, 276–280 (2021).
19. Nair, A. B. & Jacob, S. A simple practice guide for dose conversion between animals and human. *J. Basic Clin. Pharm.* **7**, 27–31 (2016).
20. Buschmann, M. D. et al. Nanomaterial delivery systems for mRNA vaccines. *Vaccines* **9**, 65 (2021).
21. Vogel, A. B. et al. BNT162b vaccines protect rhesus macaques from SARS-CoV-2. *Nature* **592**, 283–289 (2021).
22. Arunachalam, P. S. et al. T cell-inducing vaccine durably prevents mucosal SHIV infection even with lower neutralizing antibody titers. *Nat. Med.* **26**, 932–940 (2020).
23. Schenkel, J. M. et al. T cell memory. Resident memory $CD8^+$ T cells trigger protective innate and adaptive immune responses. *Science* **346**, 98–101 (2014).
24. Israelow, B. et al. Adaptive immune determinants of viral clearance and protection in mouse models of SARS-CoV-2. *Sci. Immunol.* **6**, eabl4509 (2021).
25. Pulendran, B. Learning immunology from the yellow fever vaccine: innate immunity to systems vaccinology. *Nat. Rev. Immunol.* **9**, 741–747 (2009).
26. Querec, T. et al. Yellow fever vaccine YF-17D activates multiple dendritic cell subsets via TLR2, 7, 8 and 9 to stimulate polyvalent immunity. *J. Exp. Med.* **203**, 413–424 (2006).
27. Querec, T. D. et al. Systems biology approach predicts immunogenicity of the yellow fever vaccine in humans. *Nat. Immunol.* **10**, 116–125 (2009).
28. Lee, A. et al. A molecular atlas of innate immunity to adjuvanted and live attenuated vaccines, in mice. *Nat. Commun.* **13**, 549 (2022).
29. Wimmers, F. et al. The single-cell epigenomic and transcriptional landscape of immunity to influenza vaccination. *Cell* **184**, 3915–3935 (2021).
30. Pardi, N., Hogan, M. J., Porter, F. W. & Weissman, D. mRNA vaccines—a new era in vaccinology. *Nat. Rev. Drug Discov.* **17**, 261–279 (2018).
31. Lindsay, K. E. et al. Visualization of early events in mRNA vaccine delivery in non-human primates via PET-CT and near-infrared imaging. *Nat. Biomed. Eng.* **3**, 371–380 (2019).
32. Iwasaki, A. & Medzhitov, R. Toll-like receptor control of the adaptive immune responses. *Nat. Immunol.* **5**, 987–995 (2004).
33. Alexopoulou, L., Holt, A. C., Medzhitov, R. & Flavell, R. A. Recognition of double-stranded RNA and activation of NF-κB by Toll-like receptor 3. *Nature* **413**, 732–738 (2001).
34. Diebold, S. S., Kaisho, T., Hemmi, H. & Akira, S. & Reis e Sousa, C. Innate antiviral responses by means of TLR7-mediated recognition of single-stranded RNA. *Science* **303**, 1529–1531 (2004).
35. Heil, F. et al. Species-specific recognition of single-stranded RNA via toll-like receptor 7 and 8. *Science* **303**, 1526–1529 (2004).
36. Zhao, Y. et al. SARS-CoV-2 spike protein interacts with and activates TLR4. *Cell Res.* **31**, 825 (2021).
37. Zheng, M. et al. TLR2 senses the SARS-CoV-2 envelope protein to produce inflammatory cytokines. *Nat. Immunol.* **22**, 829–838 (2021).
38. Oh, J. Z. et al. TLR5-mediated sensing of gut microbiota is necessary for antibody responses to seasonal influenza vaccination. *Immunity* **41**, 478–492 (2014).
39. Deets, K. A. & Vance, R. E. Inflammasomes and adaptive immune responses. *Nat. Immunol.* **22**, 412–422 (2021).
40. Pulendran, B., S Arunachalam, P. & O'Hagan, D. T. Emerging concepts in the science of vaccine adjuvants. *Nat. Rev. Drug Discov.* **20**, 454–475 (2021).
41. Sun, L., Wu, J., Du, F., Chen, X. & Chen, Z. J. Cyclic GMP-AMP synthase is a cytosolic DNA sensor that activates the type I interferon pathway. *Science* **339**, 786–791 (2013).
42. Ishikawa, H. & Barber, G. N. STING is an endoplasmic reticulum adaptor that facilitates innate immune signalling. *Nature* **455**, 674–678 (2008).
43. Kim, E. H. et al. Squalene emulsion-based vaccine adjuvants stimulate CD8 T cell, but not antibody responses, through a RIPK3-dependent pathway. *Elife* **9**, e52687 (2020).
44. Rehwinkel, J. & Gack, M. U. RIG-I-like receptors: their regulation and roles in RNA sensing. *Nat. Rev. Immunol.* **20**, 537–551 (2020).
45. Kato, H. et al. Differential roles of MDA5 and RIG-I helicases in the recognition of RNA viruses. *Nature* **441**, 101–105 (2006).

46. Kolumam, G. A., Thomas, S., Thompson, L. J., Sprent, J. & Murali-Krishna, K. Type I interferons act directly on CD8$^+$ T cells to allow clonal expansion and memory formation in response to viral infection. *J. Exp. Med.* **202**, 637–650 (2005).
47. Welsh, R. M., Bahl, K., Marshall, H. D. & Urban, S. L. Type 1 interferons and antiviral CD8$^+$ T cell responses. *PLoS Pathog.* **8**, e1002352 (2012).
48. Hildner, K. et al. Batf3 deficiency reveals a critical role for CD8α$^+$ dendritic cells in cytotoxic T cell immunity. *Science* **322**, 1097–1100 (2008).
49. Ravindran, R. et al. The amino acid sensor GCN2 controls gut inflammation by inhibiting inflammasome activation. *Nature* **531**, 523–527 (2016).
50. Zhang, D. W. et al. RIP3, an energy metabolism regulator that switches TNF-induced cell death from apoptosis to necrosis. *Science* **325**, 332–336 (2009).
51. Cho, Y. S. et al. Phosphorylation-driven assembly of the RIP1–RIP3 complex regulates programmed necrosis and virus-induced inflammation. *Cell* **137**, 1112–1123 (2009).
52. Shi, J. et al. Cleavage of GSDMD by inflammatory caspases determines pyroptotic cell death. *Nature* **526**, 660–665 (2015).
53. Wang, Y., Cella, M., Gilfillan, S. & Colonna, M. Cutting edge: polyinosinic:polycytidylic acid boosts the generation of memory CD8$^+$ T cells through melanoma differentiation-associated protein 5 expressed in stromal cells. *J. Immunol.* **184**, 2751–2755 (2010).
54. Wu, B. et al. Structural basis for dsRNA recognition, filament formation, and antiviral signal activation by MDA5. *Cell* **152**, 276–289 (2013).
55. Corbett, K. S. et al. SARS-CoV-2 mRNA vaccine design enabled by prototype pathogen preparedness. *Nature* **586**, 567–571 (2020).
56. Kalnin, K. V. et al. Immunogenicity and efficacy of mRNA COVID-19 vaccine MRT5500 in preclinical animal models. *NPJ Vaccines* **6**, 61 (2021).
57. Alameh, M. G. et al. Lipid nanoparticles enhance the efficacy of mRNA and protein subunit vaccines by inducing robust T follicular helper cell and humoral responses. *Immunity* **54**, 2877–2892 (2021).
58. Pulendran, B. & Davis, M. M. The science and medicine of human immunology. *Science* **369**, eaay4014 (2020).
59. Davis, M. M. A prescription for human immunology. *Immunity* **29**, 835–838 (2008).
60. Mestas, J. & Hughes, C. C. Of mice and not men: differences between mouse and human immunology. *J. Immunol.* **172**, 2731–2738 (2004).

## Methods

**Mice and immunization.** C57BL/6, B6129SF2/J, *Tlr2*$^{-/-}$, *Tlr3*$^{-/-}$, *Tlr4*$^{-/-}$, *Tlr5*$^{-/-}$ and *Tlr7*$^{-/-}$ mice were purchased from Jackson Laboratories. *Ripk3*$^{-/-}$ and *Gsdmd*$^{-/-}$ mice and littermates were gifts from Genentech (A. Gitlin). *Ifnar1*$^{-/-}$, *Mda5*$^{-/-}$, *Sting*$^{-/-}$, *cGas*$^{-/-}$ and *Batf3*$^{-/-}$ mice were bred in our animal facility at Stanford University. *Asc*$^{-/-}$ and *Nlrp3*$^{-/-}$ mice were initially obtained from Genentech (V. Dixit) and maintained in our private colony at Jackson Laboratories. *Tlr3*$^{-/-}$ mice are on the B6129SF2/J background, while other strains are on C57BL/6 background. Mice were matched for sex and aged between 8 and 14 weeks.

Discarded remnant material (Pfizer/BioNTech) was used within manufacturer's guidelines for stability at 50 µl of BNT162b2 mRNA vaccine (5 or 0.2 µg per mouse), as described in previous study[61]. In addition, because this was not available for purchase and as only remnant (otherwise to be discarded) material could be used at the time (as the product was approved for emergency use authorization only), we obtained approval from the Dean of Research at Stanford, Office for General Counsel at Stanford, and the FDA-Center for Biologics Evaluation and Research vaccines division). For immunization, mice were injected intramuscularly with 50 µl of BNT162b2 mRNA vaccine (5 or 0.2 µg per mouse) or subcutaneously at the base of the tail with 100 µl of $10^6$ plaque-forming units of YF-17D. All mice in this study were maintained under specific pathogen-free conditions, a 12-h light/12-h dark cycle and temperatures of ~18–23 °C with 40–60% humidity, and were handled according to the protocol approved by the Institutional Animal Care and Use Committee of Stanford University.

**Flow cytometry analysis of innate cells.** Draining iliac lymph nodes from BNT162b2-immunized mice and draining inguinal lymph nodes from YF-17D-immunized mice, along with whole lung or spleen, were collected and digested with 1 mg ml$^{-1}$ collagenase type IV (Worthington) for 20 min at 37 °C, followed by smashing with a 100-µm strainer to make a single-cell suspension. Red blood cells from the lung and spleen were lysed before staining. Single-cell samples were then stained with Zombie UV (1:300 dilution; BUV496; BioLegend, 423107), anti-Ly6C (1:500 dilution; BV780; BioLegend, 128041), anti-Ly6G (1:400 dilution; APC-Cy7; BioLegend, 127624), anti-CD19 (1:100 dilution; BB700; BD, 566411), anti-CD3 (1:100 dilution; BB700; BD, 742175), anti-MHCII (1:400 dilution; AF700; eBioscience, 56-5321-82), anti-CD11b (1:100 dilution; BV650; BioLegend, 101239), anti-CD11c (1:400 dilution; BV421; BioLegend, 117330), anti-CD86 (1:300 dilution; A647; BioLegend, 105020), anti-Siglec-F (1:400, PE-CF594; BD, 562757), anti-CD45 (1:200 dilution; BV610; BioLegend, 103140), anti-CD169 (1:200 dilution; PE-Cy7; BioLegend, 142412), anti-PDCA-1 (1:200 dilution; BUV563; BD, 749275), anti-CD8a (1:200 dilution; BUV805; BD, 612898), anti-CD103 (1:100 dilution; PE; eBioscience, 12-1031-82), anti-NK1.1 (1:200 dilution; BV510; BioLegend, 108738) and anti-F4/80 (1:100 dilution; BUV737; BD, 749283). Data were collected on a BD FACSymphony analyzer with BD FACSDiva (v8.0.1).

**Flow cytometry analysis of GC B, $T_{FH}$ and plasma cells in lymph nodes.** dLNs were collected and smashed with a 100-µm strainer to make a single-cell suspension followed by staining for viability with Ghost Dye Violet 510 (Tonbo Biosciences) for 5 min on ice in 1× PBS-2 mM EDTA. After washing out viability dye, cells were blocked with Fc receptor antibody α-CD16/32 (clone 2.4G2, BD) for 5 min on ice before staining with fluorochrome-conjugated antibodies in FACS staining buffer (1× PBS, 3% FBS, 1 mM EDTA, 0.02% sodium azide): CD3 (1:50 dilution; clone 17A2, BioLegend), CD4 (1:200 dilution; clone GK1.5, BioLegend), CXCR5 (1:50 dilution; clone L138D7, BioLegend), PD1 (1:200 dilution; clone 29F.1A12, BioLegend), CD19 (1:200 dilution; clone 6D5/CD19, BioLegend), CD95 (1:200 dilution; clone Jo2, BD Biosciences), CD38 (1:200 dilution; clone 90, BioLegend), CD44 (1:300 dilution; clone IM7, BioLegend) and CD138 (1:200 dilution; clone 281-2; BD Biosciences). Surface staining was carried out for 30 min on ice followed by fixation for 10 min in room temperature. Data were acquired in LSR-II and analyzed using FlowJo analysis software v10.

**Intracellular cytokine staining assay.** Whole spleen and lung samples were collected 42 d after prime (21 d after boost). Briefly, mononuclear populations from the lung were isolated from the interphase of a 70–40% Percoll gradient of single suspension prepared by enzymatic digestion with 1 mg ml$^{-1}$ type IV collagenase and DNase I. Single-cell suspensions from the spleen were prepared without digestion. Cells were plated at ~$2\times10^6$ cells per well in 96-well U-shaped plates and restimulated with S-specific overlapping peptide pools (1 µg ml$^{-1}$ of each peptide) in complete RPMI 1640 medium for overnight incubation at 37 °C in the presence of brefeldin-A (10 µg ml$^{-1}$). At day 2, cells were stained with Ghost Dye Violet 510 (Tonbo Biosciences) for 10 min on ice in 1× PBS-2 mM EDTA. After washing out viability dye, cells were blocked with Fc receptor antibody α-CD16/32 (clone 2.4G2, BD) for 5 min on ice before staining with fluorochrome-conjugated antibodies in FACS staining buffer (1× PBS, 2% FBS): CD3 (1:50 dilution; clone 145-2C11, BioLegend), CD8α (1:200 dilution; clone 53-6.7, BioLegend), CD4 (1:200 dilution; clone RM4-5, BioLegend), CD44 (1:400 dilution; clone IM7, BioLegend), CD69 (1:200 dilution; clone H1.2F3; BioLegend) and CD45 (1:200 dilution; clone 30-F11, BioLegend). Cells were incubated for 30 min on ice for surface staining followed by fixation and permeabilization in BD Fix/Perm buffer and then stained intracellularly with fluorochrome-conjugated antibodies in Fix/Perm buffer: IFN-γ (1:100 dilution; clone XMG1.2, BioLegend), TNF (1:100 dilution; clone MP6-XT22, BioLegend), IL-2 (1:100 dilution; clone JES6-5H4, BioLegend) and IL-4 (1:100 dilution; clone 11B11, BioLegend) per the manufacturer's recommendation. Data were acquired in LSR-II and analyzed using FlowJo v10.

**Antigen-specific tetramer and tissue-resident memory T cell staining.** After staining cells with viability dye, cells were surface stained with anti-CD3 (1:50 dilution; clone 145-2C11, BioLegend), CD8α (1:200 dilution; clone 53-6.7, BioLegend), CD4 (1:200 dilution; clone RM4-5, BioLegend), CD44 (1:400 dilution; clone IM7, BioLegend), CD45 (1:200 dilution; clone 30-F11, BioLegend), CD69 (1:200 dilution; clone H1.2F3, BioLegend), CD103 (1:200 dilution; clone 2E7, BioLegend) and Spike S-specific Tetramer (1:200 dilution; residues 539–546, VNFNFNGL, H-2K(B)), followed by fixation. Data were acquired in LSR-II and analyzed with FlowJo v10.

**Flow cytometry analysis of IFN-γ-producing cells in lymph nodes.** After staining cells with viability dye, cells were surface stained with anti-CD3 (clone 145-2C11, BioLegend), CD8α (clone 53-6.7, BioLegend), CD4 (clone RM4-5, BioLegend), CD44 (clone IM7, BioLegend), CD45 (clone 30-F11, BioLegend), NK1.1 (clone PK136, BioLegend) and TCR delta (1:100 dilution; clone Gl3, BioLegend), fixed and permeabilized in BD Fix/Perm buffer, and stained intracellularly with anti-IFN-γ (XMG1.2, BioLegend) according to the manufacturer's recommendation. Data were acquired in LSR-II and analyzed with FlowJo v10. To block IFN-γ receptor, 1 mg per mouse of IFN-γ receptor neutralizing antibody (clone 2E2, BioXCell, BE0287) or isotype control (IgG, BioXCell, BE0091) was given intraperitoneally on days 19, 20 and 21 after prime. Then, mice were boosted at day 21 after prime, and lymph nodes were collected at day 1 after boost. To delete T cells or NK cells, 0.3 mg per mouse of anti-mouse CD8 (clone YTS 169.4, BioXCell, BE0117), anti-mouse CD4 (clone GK1.5, BioXCell, BE0003-1) or anti-mouse NK1.1 (clone PK136, BioXCell, BE0036) or isotype control (clone LTF-2, BioXCell, BE0090 for anti-CD4/CD8; or clone C1.18.4, BioXCell, BE0085 for anti-NK1.1) was given intraperitoneally on day 20 after priming. Mice were boosted at day 21. Serum IFN-γ levels and innate cell activation in spleen were checked at day 22.

**Luminex assay.** The assay was performed by the Human Immune Monitoring Center at Stanford University. Mouse 48-plex Procarta kits (EPX480-20834-901) were purchased from Thermo Fisher and used according to the manufacturer's recommendations with modifications as described below. Beads were added to a 96-well plate and washed in a BioTek ELx405 washer. Samples were added to the plate containing the mixed antibody-linked beads and incubated overnight at 4 °C with shaking. Cold (4 °C) and room temperature incubation steps were performed on an orbital shaker at 500–600 r.p.m. Following the overnight incubation, plates were washed in a BioTek ELx405 washer and biotinylated detection antibody was added for 60 min at room temperature with shaking. Plates were washed as described above and streptavidin-PE was added. After incubation for 30 min at room temperature, a wash was performed as above and reading buffer was added to the wells. Each sample was measured in singlets. Plates were read on a FM3D FlexMap instrument with a lower bound of 50 beads per sample per cytokine/chemokine. Custom Assay Chex control beads were purchased from Radix BioSolutions, and were added to all wells.

**Anti-spike binding ELISA.** SARS-CoV-2 spike protein was purchased from Sino Biologicals (40589-V08B1). High-binding 96-well plates were coated with 100 ng of spike protein diluted at a concentration of 2 mg ml$^{-1}$ in PBS. The plates were washed once and blocked with 3% non-fat milk for 1 h at room temperature. Sera samples serially diluted in 1% non-fat milk containing PBS were added to the plates and incubated at 37 °C for 1 h. The plates were washed 3× with PBS-T, and horseradish peroxidase-conjugated goat anti-mouse IgG, IgG1 or IgG2c (SouthernBiotech, 1:6,000 dilution) in PBS-T containing 1% non-fat milk was added and incubated for 1 h at room temperature. Wells were washed three times with PBS-T before addition of 3,3′,5,5′-tetramethylbenzidine substrate solution (Thermo Pierce). The reaction was stopped after 3 min by addition of 0.16 M sulfuric acid. The optical density at 450 nm was measured with a Bio-Rad microplate reader.

**Pseudotyped lentivirus virus production.** Viral transfections were done in HEK293T cells using Bio T transfection reagent. Five million cells were seeded in D10 medium (DMEM + 10% FBS, L-glutamate, penicillin, streptomycin and 10 mM HEPES) in 10-cm plates 1 d before transfection. A five-plasmid system[62] was used for viral production. The spike vector contained the 21 amino acid truncated form of the SARS-CoV-2 spike sequence from the Wuhan-Hu-1 strain of SARS-CoV-2. Plasmids were added to D10 medium in the following ratios: 10 µg pHAGE-Luc2-IRS-ZsGreen, 3.4 µg FL spike, 2.2 µg HDM-Hgpm2, 2.2 µg HDM-Tat1b and 2.2 µg pRC-CMV-Rev1b in a final volume of 1 ml; 30 µl of Bio T was then added. Transfection reactions were incubated for 10 min at room temperature, and then added up to 10 ml with D10 medium. This mixture was added slowly to plated cells. Culture medium was removed 24 h after transfection

and replaced with fresh D10 medium. Viral supernatants were collected 72 h after transfection by spinning at 300*g* for 5 min followed by filtering through a 0.45-µm filter. Viral stocks were aliquoted and stored at −80 °C until ready for use.

**Neutralization assay.** The target cells used for infection in viral neutralization assays were from a HeLa cell line stably overexpressing the SARS-CoV-2 receptor, ACE2, as well as the protease known to process SARS-CoV-2, TMPRSS2 (ref. [63]). ACE2/TMPRSS2/HeLa cells were plated 1 d before infection at 5,000 cells per well or 2 d before infection at 2,500 cells per well. White-walled, clear-bottom, 96-well plates were used for the assay (Thermo Fisher Scientific). On the day of the assay, dilutions of serum were made into sterile D10 medium to a final volume of 30 µl. Samples were run in technical duplicate in each experiment. All other wells contained only D10 medium. A virus mixture was made containing the virus of interest (for example, SARS-CoV-2 with a 21 amino acid deletion on the C terminus), D10 medium (DMEM + 10% FBS, L-glutamine, 100 U $ml^{-1}$ penicillin, 100 U $ml^{-1}$ streptomycin and 10 mM HEPES) and polybrene. Virus dilutions into medium were selected such that a suitable signal would be obtained in the virus-only wells. A suitable signal was selected such that the virus-only wells would achieve a luminescence of at least >10,000 relative light units. Sixty microliters of this virus mixture was added to each of the serum dilutions to make a final volume of 120 µl in each well. Virus-only wells were made containing 60 µl D10 medium and 60 µl virus mixture. Cell-only wells were made containing 120 µl of D10 medium. The diluted serum/virus mixture was left to incubate for 1 h at 37 °C. Following incubation, the medium was removed from the cells on the plates made 1 or 2 d before, replaced with 100 µl of diluted serum/virus dilutions, and incubated at 37 °C for approximately 48 h. Infectivity readout was performed by measuring luciferase with a microplate reader (BioTek). Normalized values were fit with a three-parameter nonlinear regression inhibitor curve in GraphPad Prism (v9.2.0) to obtain $NT_{50}$ (half neutralizing antibody titer) values.

**Spike protein detection in serum.** SARS-CoV-2 (2019-nCoV) Spike Detection ELISA Kit (Sino Biological, KIT40591) was used to measure spike protein in mouse serum according to the manufacturer's protocol. First, plates were washed three times followed by the addition of standard and diluted samples (2 µl mouse serum was added into 98 µl dilution buffer). Plates were then incubated for 2 h. After incubation, plates were washed three times and incubated with detection antibody for 1 h. Again, the plates were washed three times and 200 µl of substrate solution were added for 20 min. Finally, 50 µl stop solution were added and the optical density at 450 nm was measured with a microplate reader (Bio-Rad). All incubations were conducted at room temperature.

**Spike mRNA vaccine detection by RT–PCR.** Tissues were taken at day 1 after immunization. Tissues were weighted and homogenized with a bead miller (Fisher). Total RNA was purified with a PureLink RNA mini kit (Invitrogen). RNA purified from BNT162b2 mRNA vaccine was diluted serially and served as the standard. A Luna universal probe one-step RT–PCR kit (NEB) was used to measure the cycle threshold (Ct) of purified RNA with mRNA vaccine-specific primers (mVac-F: 5′-TACCAAGCTGAACGACCTGT, mVac-R: 5′-TTGCTGTTC CAGGCAATCAC, mVac-Probe: 5′-FAM-TGCCCGACGACTTCACCGGC-IBFQ).

**IFN-γ, IFN-α and damage-associated molecular pattern signal detection.** Serum IFN-γ and IFN-α levels were determined in serum samples by ELISA. Serum IFN-γ was detected with the Quantikine ELISA kit (R&D Systems, MIF00). IFN-α in serum was measured using ELISA sets (PBL, 421201). HMGB1 was detected with the Chemiluminescence ELISA kit (Novus Biologicals, NBP262782). ELISAs were performed according to the manufacturers' instructions. Serum double-stranded DNA concentrations were determined with a Quant-iT PicoGreen dsDNA Kit (Invitrogen, P11496). Uric acid in serum was measured with a Uric Acid Assay Kit (Abcam, ab65344).

**scRNA-seq samples and preparation.** Draining iliac lymph nodes from BNT162b2-immunized mice and draining inguinal lymph nodes from YF-17D-immunized mice were collected and digested into single-cell suspensions. One million total cells were set aside on ice. The rest of the cells were incubated with biotinylated CD3, CD19 and NK1.1 antibodies on ice for 20 min. Streptavidin-labeled magnetic beads (BD IMag Streptavidin Particles Plus-DM) were added and incubated on ice for 30 min. Unbonded cells were collected and $CD11b^+$ myeloid cells, pDCs ($CD11c^{lo}CD11b^-$PDCA-1+) and DCs ($CD11c^+$MHC-$II^+$) were sorted with flow cytometry. Sorted cells were combined with total lymphocytes at a 1:1 ratio and resuspended in cold PBS supplemented with 1% BSA (Miltenyi) and 0.5 U $µl^{-1}$ RNase Inhibitor (Sigma Aldrich). Cells were partitioned into gel beads-in emulsion (GEMs) using the 10x Chromium 3′ V3 chemistry system (10x Genomics). The released RNA was reverse transcribed in the C1000 touch PCR instrument (Bio-Rad), in accordance with the manufacturer's recommendations. Barcoded cDNA was extracted from the GEMs by post-GEM RT-Cleanup and amplified for 12 cycles. Amplified cDNA was subjected to 0.6x SPRI beads cleanup (Beckman, B23318). Twenty five percent of the amplified cDNA was subjected to enzymatic fragmentation, end repair, A-tailing, adaptor ligation and 10X specific sample indexing per the manufacturer's protocol. Sequencing libraries were generated and the quality was assessed through Bioanalyzer (Agilent) analysis. Libraries were pooled and sequenced on the HiSeq 4000 instrument (Illumina) with a targeted read depth of 40,000 read pairs per cell.

**scRNA-seq data analysis.** Cell Ranger v3.1.0 (10x Genomics) was used to quantify transcript levels against the 10x Genomics GRCh38 reference (v3.0.0). Raw count data were filtered to remove cells with a mitochondrial RNA fraction of >20% of total RNA counts per cell, cells with <100 unique features or cells with <200 total reads. The filtered count matrix was used to create a Seurat[64] (v3.1.4) object. Filtered read counts were scaled by a factor of 10,000 and log transformed. Doublets were identified with scds[65] (v1.2.0); cells with a doublet score in the top decile were removed. The remaining 52,788 cells were processed with the default Seurat pipeline. Specifically, the most variable 2,000 RNA features were used to perform principal-component analysis on the log-transformed counts. The first 25 components were used for further downstream analyses, including clustering and UMAP projections. Clusters were identified with Seurat SNN graph construction followed by Louvain community detection on the resultant graph with a resolution of 0.2, yielding 20 clusters. Differential expression for each time point compared to the baseline was calculated with a Wilcoxon rank-sum test. Gene-set enrichment analysis was run using all genes ranked by Wald statistic.

Macrophage clusters C2 and C15 were re-embedded using genes that characterized an epigenetically remodeled monocyte population enriched in humans 21 d after vaccination with two doses of H5N1/AS03 (ref. [29]). Principal components were calculated from the most variable genes within this set; Louvain community detection was again used with a resolution of 0.2 to determine cluster identity. Complex Heatmap (v2.2.0) was used for all heat maps. All analysis was performed in R (v3.6.3).

**Quantification and statistical analysis.** scRNA-seq statistical analysis was completed as described above. All other statistical analysis was performed with Prism (GraphPad Software v9.2.0). For comparing two groups, *P* values were determined using Student's *t*-tests (two-tailed). For comparing more than two groups, one-way ANOVAs followed by Tukey's test were applied. Differences between groups were considered significant for $P$ values $< 0.05$. No statistical methods were used to predetermine sample sizes, but our sample sizes are similar to those reported in previous publications[38,43]. Mice were assigned to the various experimental groups randomly. Data collection and analysis were not performed blind to the conditions of the experiments. Data distribution was assumed to be normal, but this was not formally tested. No data points were excluded from the analyses.

**Reporting Summary.** Further information on research design is available in the Nature Research Reporting Summary linked to this article.

## Data availability

Single-cell RNA-seq data are publicly accessible in the Gene Expression Omnibus under accession code GSE179131. All analyses and visualizations were performed in R (v3.6.3). Source data are provided with this paper.

## Code availability

Computer code is available upon reasonable request.

## References

61. Warren, C. M. et al. Assessment of allergic and anaphylactic reactions to mRNA COVID-19 vaccines with confirmatory testing in a US regional health system. *JAMA Netw. Open* **4**, e2125524 (2021).
62. Crawford, K. H. D. et al. Protocol and reagents for pseudotyping lentiviral particles with SARS-CoV-2 spike protein for neutralization assays. *Viruses* **12**, 513 (2020).
63. Rogers, T. F. et al. Isolation of potent SARS-CoV-2 neutralizing antibodies and protection from disease in a small animal model. *Science* **369**, 956–963 (2020).
64. Stuart, T. et al. Comprehensive integration of single-cell data. *Cell* **177**, 1888–1902 (2019).
65. Bais, A. S. & Kostka, D. scds: computational annotation of doublets in single-cell RNA-sequencing data. *Bioinformatics* **36**, 1150–1158 (2020).

## Acknowledgements

We thank Ed Mockarski and Pratyusha Mandal for their advice and help during the early stages of this work. We thank the technical support from the Stanford Shared FACS Facility. Sorting was performed on an instrument in the Shared FACS Facility purchased by Parker Institute for Cancer Immunotherapy (PICI). We thank D. Wagh from Stanford Functional Genomics for preparing the single-cell library construction. We thank L. Witt, B. Betts and T. Chang from Stanford Health care system for providing remnant vaccines. We thank the National Institutes of Health tetramer core facility for providing the spike-specific tetramer for $CD8^+$ T cell detection. We thank B. Franco from Stanford Veterinary Service Center (VSC) for technical support. The study was supported by NIH grants (R37 DK057665, R37 AI048638, U19 AI090023 and U19 AI057266 to R. Ahmed;

U19 AI159840 to S. Foung), the Bill and Melinda Gates Foundation, and the Soffer Fund endowment and Open Philanthropy to B.P.

## Author contributions

C.L., P.S.A. and B.P. designed research, interpreted data and wrote the manuscript. C.L. organized and led the research and analyzed the data. A.L. helped with innate cells staining. L.G., M.T., J.Z.A., R.V., N.R. and Y.F. helped with T cell analysis. M.K.S. performed the scRNA-seq data analysis. F.W. and A.L. helped to prepare samples for scRNA-seq. M.S. and P.A.W. conducted neutralization assays. E.V., Y.W. and M.T. took care of mice. D.D., R.H. and H.P. helped to provide remnant vaccine vials. W.L., P.K., A.D.G., P.K. and K.C.N. provided the analysis tools and key resources.

## Competing interests

B.P. has served or is serving on the External Immunology Network of GSK, and on the scientific advisory boards of Sanofi, Medicago, CircBio and Boehringer-Ingelheim. A.D.G. is a visiting scientist at Genentech. The other authors declare no competing interests.

## Additional information

**Extended data** is available for this paper at https://doi.org/10.1038/s41590-022-01163-9.

**Supplementary information** The online version contains supplementary material available at https://doi.org/10.1038/s41590-022-01163-9.

**Correspondence and requests for materials** should be addressed to Bali Pulendran.

**Peer review information** *Nature Immunology* thanks Olivier Schwartz and the other, anonymous, reviewer(s) for their contribution to the peer review of this work. Primary Handling Editor: N. Bernard, in collaboration with the *Nature Immunology* team. Peer reviewer reports are available.

**Reprints and permissions information** is available at www.nature.com/reprints.

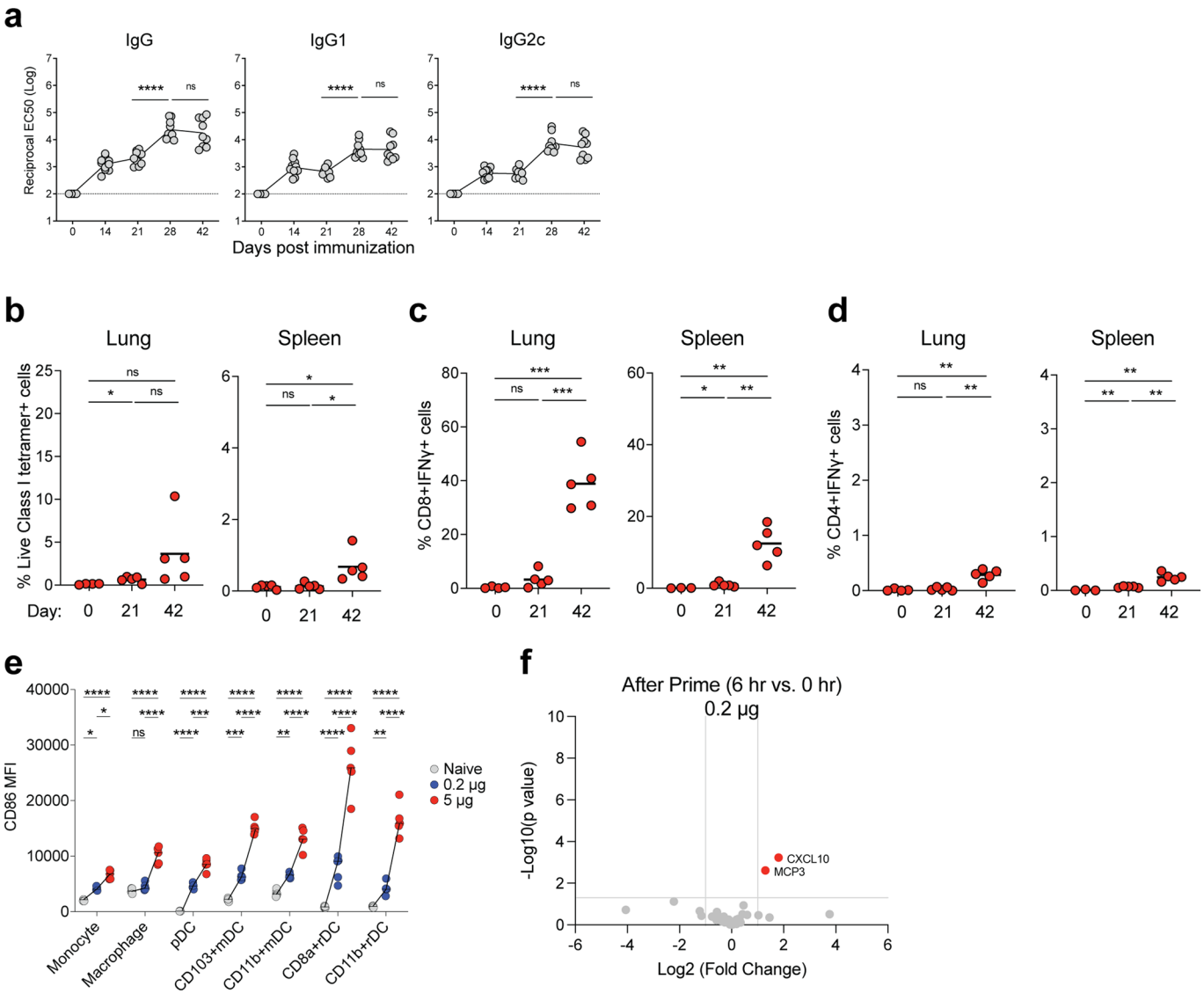


**Extended Data Fig. 1 | Immune response induced by low immunization dose in mice. a**, S binding titers induced by low dose (0.2 µg/mouse) of BNT162b2 immunization measured by ELISA. **b**, Class I tetramer specific CD8 T cell response in lung and spleen of mice measured at days 21 and 42 after BNT162b2 immunization (0.2 µg/mouse). **c-d**, Antigen specific CD8 **(c)** and CD4 **(d)** T cell response in lung and spleen of mice detected at days 21 and 42 by intracellular cytokine staining (ICS) assay. **e**, Comparison between the activation of innate cells in dLNs induced by low (0.2 µg/mouse) and high immunization doses (5 µg/mouse). **f**, Cytokines/chemokines produced at 6 h post prime with low (0.2 µg/mouse) dose detected by Luminex assay. Data were combined from two independent experiments **(a)** or one representative experiment **(b-f)**. One-Way ANOVA followed by Tukey's test was applied (a-e). P-values were determined using Student's t-tests (two-tailed) (f). *P < 0.05, **P < 0.01, ***P < 0.001, ****P < 0.0001.

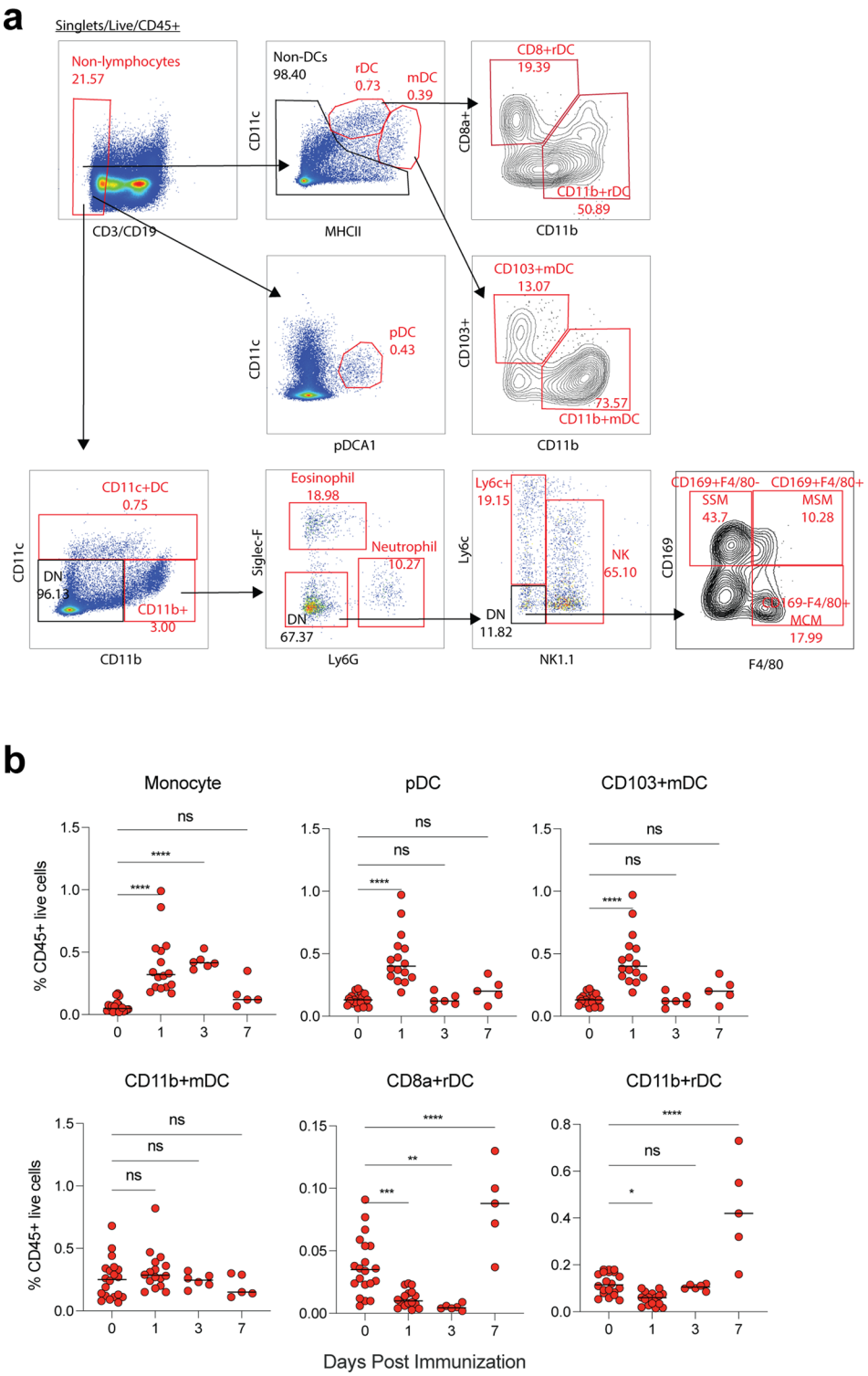


**Extended Data Fig. 2 | Innate cells activated by BNT162b2. a**, Gating strategy. **b**, Frequency of innate cells in live CD45 + cells after BNT162b2 immunization in dLNs. Data were combined from at least two independent experiments. One-Way ANOVA followed by Tukey's test was applied in (**b**). *P < 0.05, **P < 0.01, ***P < 0.001, ****P < 0.0001.

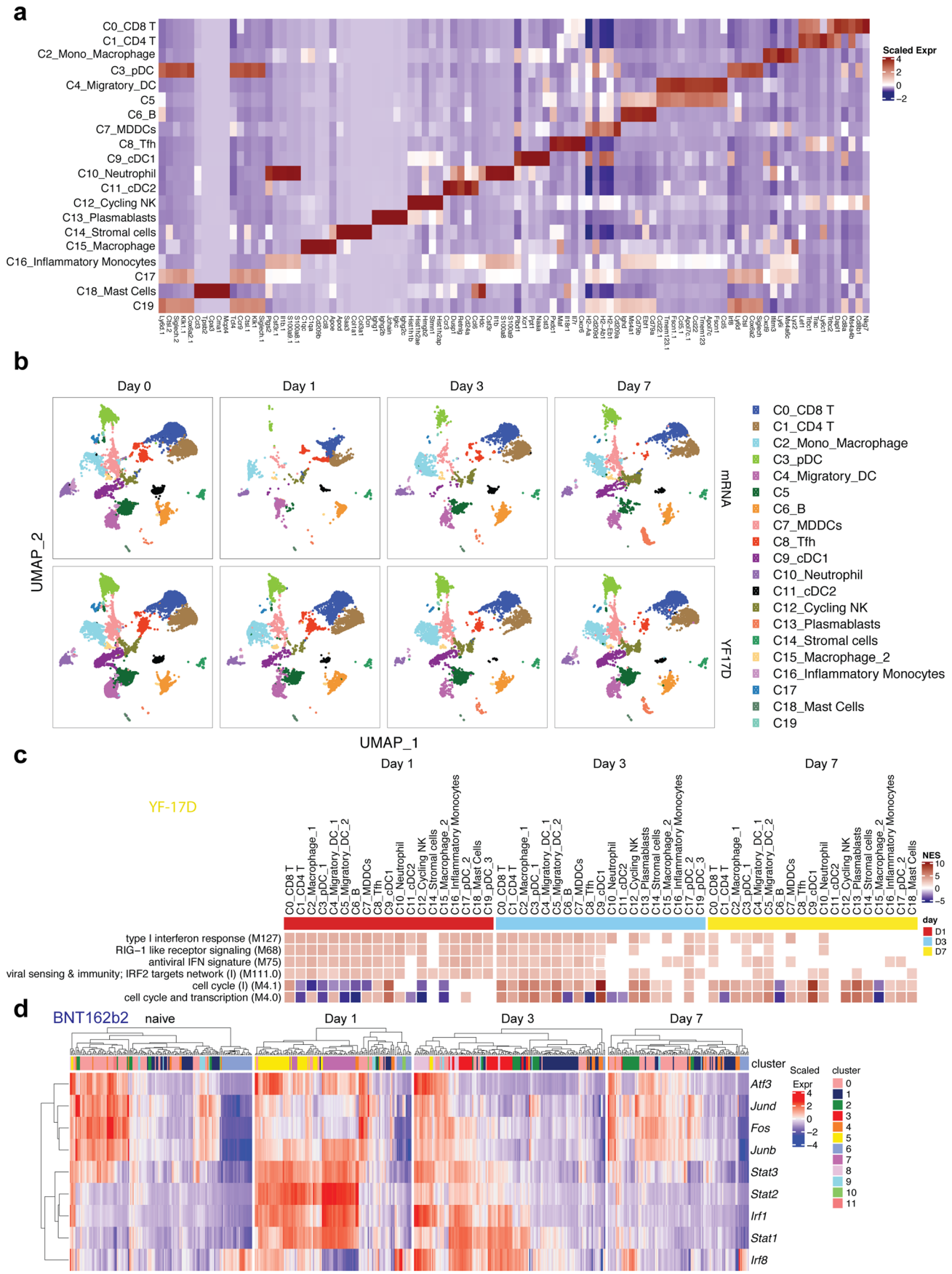


**Extended Data Fig. 3 | See next page for caption.**

**Extended Data Fig. 3 | scRNAseq analysis of immune response induced by BNT162b2 and YF-17D. a**, Clusters and their associated cluster-specific genes. **b**, UMAP of cell types clustered by single-cell transcriptional analysis at indicated time. **c**, Significantly enriched interferon BTMs (false discovery rate [FDR] < 0.05, absolute normalized enrichment score [NES] > 2) across all clusters from days 1 to 7 after YF-17D immunization. Only clusters with a significantly modulated pathway are shown. **d**, Heatmap of key interferon response and AP-1 transcription factors after BNT162b2 immunization over time. Samples used for scRNAseq were pooled from three independent experiments containing 8-10 mice.

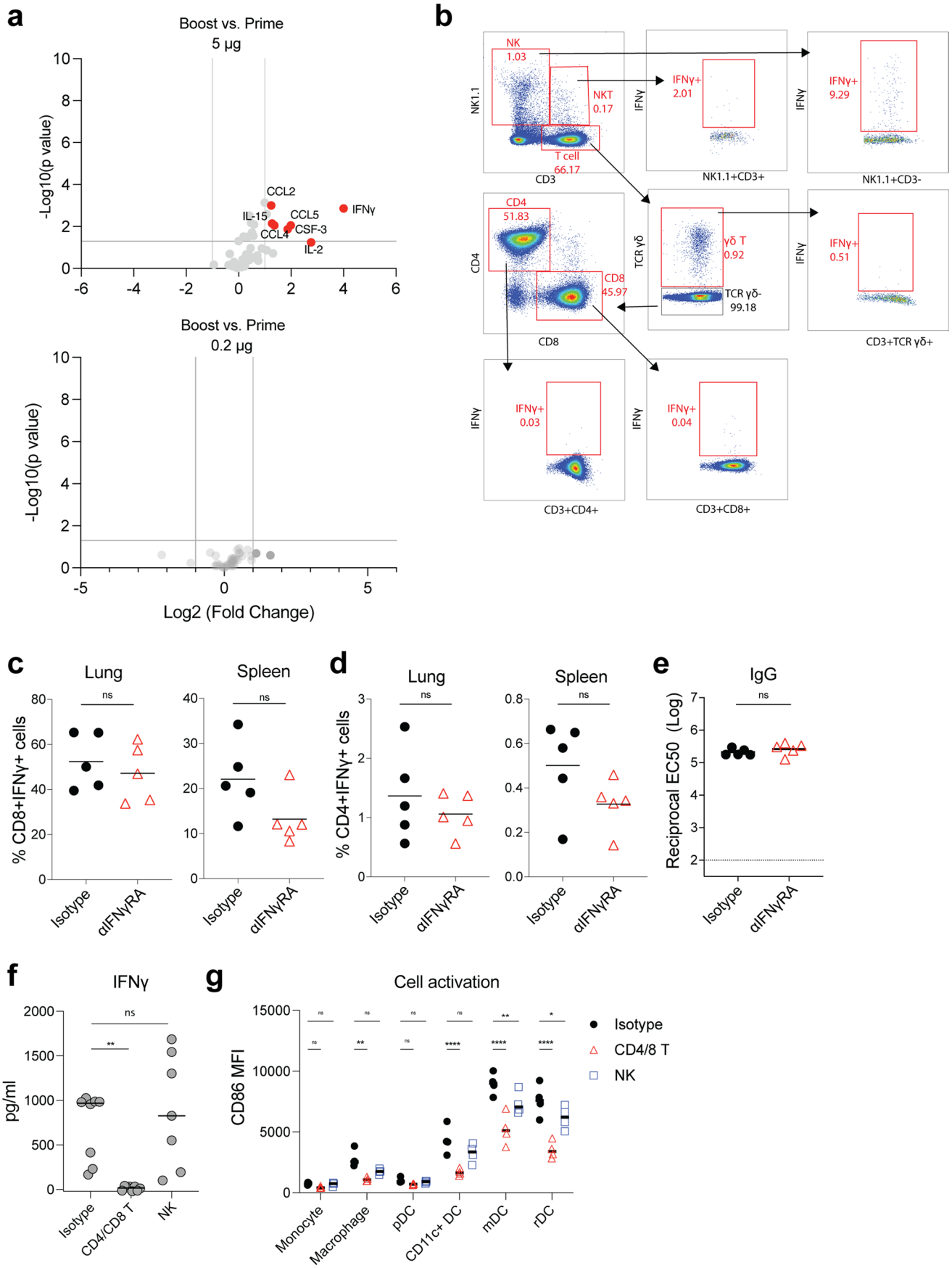


**Extended Data Fig. 4 | See next page for caption.**

**Extended Data Fig. 4 | IFNγ production after prime and boost. a**, Luminex assay of serum cytokines/chemokines at 6 h post-prime and boost with 5 μg/mouse and 0.2 μg/mouse, respectively. Data were combined from five mice for each group. **b**, Gating strategy to analyze IFNγ producing cells in dLNs. **c-e**, CD8 + and CD4 + T cell responses, and IgG titer at day 42 after blocking of IFNγ receptor. Mice were treated with IFNγ receptor neutralizing antibody or isotype control before boost at day 21. **f**, Serum IFNγ level at day 22 (1 day after boost) after T cells (CD4 and CD8 T cells) or NK cells depletion at day 21. **g**, Innate cell activation in spleen at 1 day post boost after T or NK cell depletion. P-values were determined using Student's t-tests (two-tailed) (**a, c-e**), One-Way ANOVA (**f**), or Two-way ANOVA (**g**). *$P < 0.05$, **$P < 0.01$, ***$P < 0.001$, ****$P < 0.0001$.

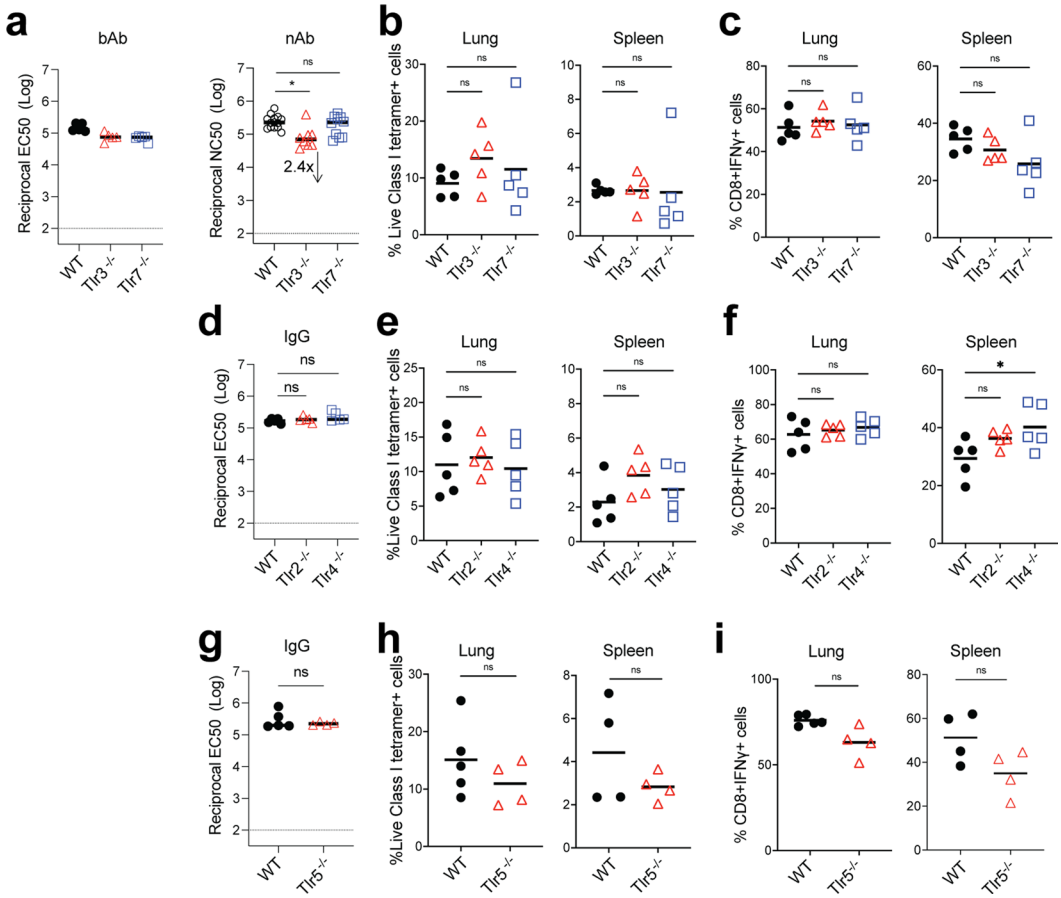


**Extended Data Fig. 5 | Roles of TLRs for BNT162b2-induced antibody and T cell response.** bAb and nAb titers of WT and *Tlr3*$^{-/-}$, *Tlr7*$^{-/-}$ **(a)**, bAb (IgG) titers of WT and *Tlr2*$^{-/-}$, *Tlr4*$^{-/-}$ **(d)**, *Tlr5*$^{-/-}$ **(g)** mice at day 42. CD8 + T cell response in WT and *Tlr3*$^{-/-}$, *Tlr7*$^{-/-}$ **(b-c)**, *Tlr2*$^{-/-}$, Tlr4$^{-/-}$ **(e-f)**, and *Tlr5*$^{-/-}$ **(h-i)** mice. Data were combined from two independent experiments. One-Way ANOVA followed by Tukey's test was applied in (**a-f**). P-values in (**g-i**) were determined using Student's t-tests (two-tailed). *P < 0.05, **P < 0.01.

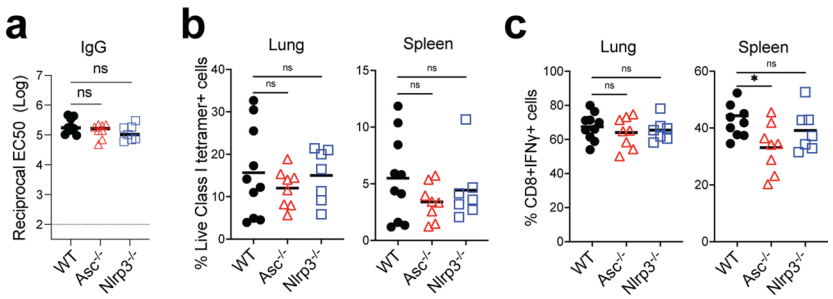


**Extended Data Fig. 6 | Roles of inflammasome for BNT162b2-induced antibody and T cell response. a**, IgG titers of WT, *Asc*$^{-/-}$, and *Nlrp3*$^{-/-}$ mice at day 42. **(b-c)**, CD8 + T cell response in WT, *Asc*$^{-/-}$, and *Nlrp3*$^{-/-}$ mice. Data were combined from two independent experiments. One-Way ANOVA followed by Tukey's test was applied. *P < 0.05.

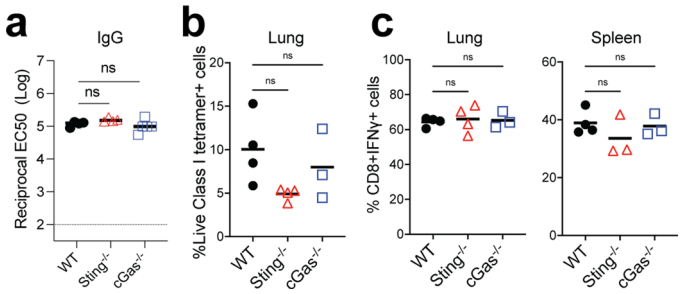


**Extended Data Fig. 7 | Role of cGAS and STING for BNT162b2-induced antibody and T cell response. a**, IgG titers of WT, *cGas*$^{-/-}$, and *Sting*$^{-/-}$ mice at day 42. **(b-c)**, CD8 + T cell response in WT, *cGas*$^{-/-}$, and *Sting*$^{-/-}$ mice. Data are one representative of two independent experiments. One-Way ANOVA followed by Tukey's test was applied.

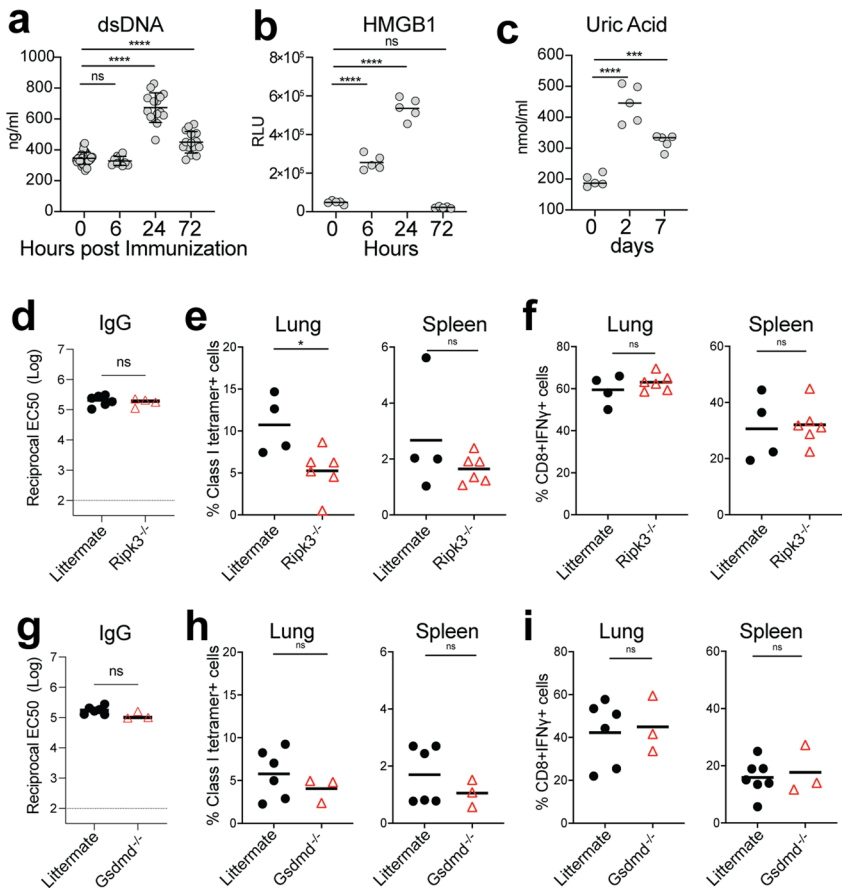


**Extended Data Fig. 8 | Role of cell death in BNT162b2-induced antibody and T cell response. a-c**, DAMP signals including dsDNA **(a)**, HMGB1 **(b)**, and uric acid **(c)** induced by BNT162b2 immunization at the indicated time. **d**, IgG titers of littermate and *Ripk3*$^{-/-}$ mice at day 42. **e-f**, CD8 + T cell response in littermate and *Ripk3*$^{-/-}$ mice. **g**, IgG titers of littermate and *Gsdmd*$^{-/-}$ mice at day 42. **h-i**, CD8 + T cell response in littermate and *Gsdmd*$^{-/-}$ mice. Data were one representative of at least two independent experiments **(a)**, or one representative experiment **(b-i)**. One-Way ANOVA followed by Tukey's test was applied in (**a-c**). P-values in (**d-i**) were determined using Student's t-tests (two-tailed). *$P < 0.05$, ***$P < 0.001$, ****$P < 0.0001$.

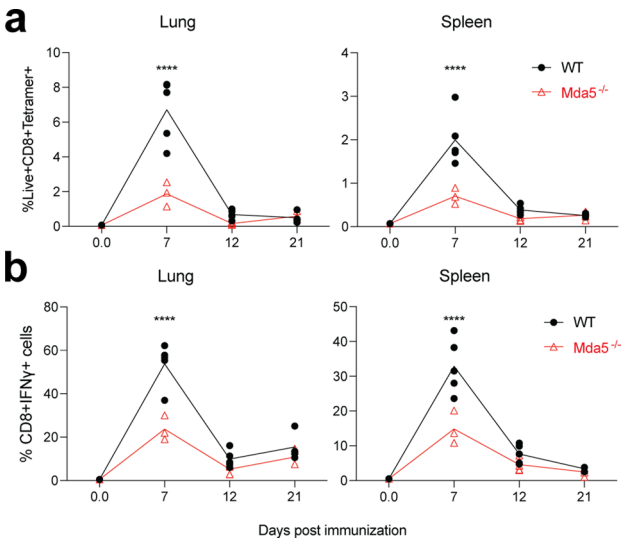


**Extended Data Fig. 9 | Role of MDA5 in BNT162b2-induced T cell response after prime. a-b**, CD8 + T cell response in WT and *Mda5*$^{-/-}$ mice at indicated time post prime. P-values were determined using two-way ANOVA. ****P < 0.0001.

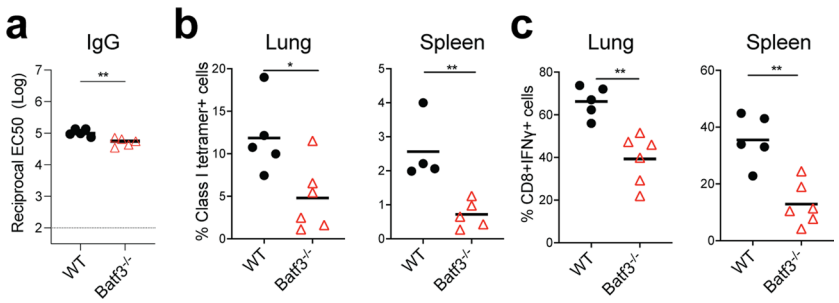


**Extended Data Fig. 10 | Role of Batf3 in BNT162b2-induced antibody and T cell response. a**, IgG titers of WT and *Batf3*$^{-/-}$ mice at day 42. **b**, CD8 + T cell response in WT and *Batf3*$^{-/-}$ mice. Data were one representative of three independent experiments. P-values were determined using Student's t-tests (two-tailed). *P < 0.05, **P < 0.01.

nature portfolio

Corresponding author(s): Bali Pulendran

Last updated by author(s): Jan 29, 2022

# Reporting Summary

Nature Portfolio wishes to improve the reproducibility of the work that we publish. This form provides structure for consistency and transparency in reporting. For further information on Nature Portfolio policies, see our Editorial Policies and the Editorial Policy Checklist.

## Statistics

For all statistical analyses, confirm that the following items are present in the figure legend, table legend, main text, or Methods section.

| n/a | Confirmed |
|---|---|
| ☐ | ☒ The exact sample size (*n*) for each experimental group/condition, given as a discrete number and unit of measurement |
| ☐ | ☒ A statement on whether measurements were taken from distinct samples or whether the same sample was measured repeatedly |
| ☐ | ☒ The statistical test(s) used AND whether they are one- or two-sided<br>*Only common tests should be described solely by name; describe more complex techniques in the Methods section.* |
| ☒ | ☐ A description of all covariates tested |
| ☐ | ☒ A description of any assumptions or corrections, such as tests of normality and adjustment for multiple comparisons |
| ☐ | ☒ A full description of the statistical parameters including central tendency (e.g. means) or other basic estimates (e.g. regression coefficient) AND variation (e.g. standard deviation) or associated estimates of uncertainty (e.g. confidence intervals) |
| ☐ | ☒ For null hypothesis testing, the test statistic (e.g. *F*, *t*, *r*) with confidence intervals, effect sizes, degrees of freedom and *P* value noted<br>*Give P values as exact values whenever suitable.* |
| ☒ | ☐ For Bayesian analysis, information on the choice of priors and Markov chain Monte Carlo settings |
| ☒ | ☐ For hierarchical and complex designs, identification of the appropriate level for tests and full reporting of outcomes |
| ☒ | ☐ Estimates of effect sizes (e.g. Cohen's *d*, Pearson's *r*), indicating how they were calculated |

*Our web collection on statistics for biologists contains articles on many of the points above.*

## Software and code

Policy information about availability of computer code

| | |
|---|---|
| Data collection | BD FACSDiva software version 8.0.1 was used for collecting the flow cytometry data on the LSRII.2 and BD FACSymphony machine. |
| Data analysis | FlowJo software v.10.0 (Treestar Inc); GraphPad Prism version 9.0.1; Adobe Illustrator 25.0. All statistical analysis are two-sided. All analyses and visualizations of sc-RNAseq data were performed in R (V3.6.3). Computer code is available upon reasonable request. |

For manuscripts utilizing custom algorithms or software that are central to the research but not yet described in published literature, software must be made available to editors and reviewers. We strongly encourage code deposition in a community repository (e.g. GitHub). See the Nature Portfolio guidelines for submitting code & software for further information.

## Data

Policy information about availability of data

All manuscripts must include a data availability statement. This statement should provide the following information, where applicable:

- Accession codes, unique identifiers, or web links for publicly available datasets
- A description of any restrictions on data availability
- For clinical datasets or third party data, please ensure that the statement adheres to our policy

Single-Cell RNAseq data are publicly accessible in the GEO under accession numbers GSE179131.

# Field-specific reporting

Please select the one below that is the best fit for your research. If you are not sure, read the appropriate sections before making your selection.

☒ Life sciences ☐ Behavioural & social sciences ☐ Ecological, evolutionary & environmental sciences

For a reference copy of the document with all sections, see nature.com/documents/nr-reporting-summary-flat.pdf

# Life sciences study design

All studies must disclose on these points even when the disclosure is negative.

| | |
|---|---|
| Sample size | No statistical test was used to determine the number of samples. Sample sizes were determined as appropriate to evaluate detection of large vaccine effects based on several studies done by us and others. |
| Data exclusions | No data were excluded from any of the analysis. |
| Replication | All the assays were repeated with biological replicates in each experiment, and all the repeats are successful. |
| Randomization | The study involved the same batch of mice (C57BL/6) that were obtained from Jackson laboratories. Mice were allocated to cages with 3-5 mice per cage, and each cage was assigned to an immunization group. |
| Blinding | All the experiments were conducted in an unblinded way since the investigators were involved in overall conduct of the study. |

# Reporting for specific materials, systems and methods

We require information from authors about some types of materials, experimental systems and methods used in many studies. Here, indicate whether each material, system or method listed is relevant to your study. If you are not sure if a list item applies to your research, read the appropriate section before selecting a response.

## Materials & experimental systems

| n/a | Involved in the study |
|---|---|
| ☐ | ☒ Antibodies |
| ☒ | ☐ Eukaryotic cell lines |
| ☒ | ☐ Palaeontology and archaeology |
| ☐ | ☒ Animals and other organisms |
| ☒ | ☐ Human research participants |
| ☒ | ☐ Clinical data |
| ☒ | ☐ Dual use research of concern |

## Methods

| n/a | Involved in the study |
|---|---|
| ☒ | ☐ ChIP-seq |
| ☐ | ☒ Flow cytometry |
| ☒ | ☐ MRI-based neuroimaging |

## Antibodies

Antibodies used

Antibody, Fluorophore, Vendor, Cat #, Clone, Lot #

anti-Ly6C, BV780, Biolegend, # 128041, HK1.4, B311364
anti-Ly6G, APC-Cy7, Biolegend, # 127624, 1A8, B294666
anti-CD19, BB700, BD, # 566411, 1D3, 0079006
anti-CD3, BB700, BD, #742175, 17A2, 0202623
anti-MHCII, AF700, eBioscience, #56-5321-82, M5/114.15.2, 2210930
anti-CD11b, BV650, Biolegend, #101239, M1/70, B335585
anti-CD11c, BV421, Biolegend, #117330, N418, B294539
anti-CD86, A647, Biolegend, #105020, GL-1, B245405
anti-Siglec-F, PE-CF594, BD, #562757, E50-2440, 0064626
anti-CD24, BUV395, BD, #744471, M1/69, 1102765
anti-CD45, BV605, Biolegend, #103140, 30-F11, B313899
anti-CD169, PE-Cy7, Biolegend, #142412, 3D6.112, B264616
anti-PDCA-1, BUV563, BD, #749275, 927, 1271522
anti-CD8a, BUV805, BD, #612898, 53-6.7, 0328533
anti-CD103, PE, eBioscience, #12-1031-82, 2E7, 2054351
anti-NK1.1, BV510, Biolegend, #108738, PK136, B326849
anti-F4/80, BUV737, BD, #749283, T45-2342, 1168211
anti CD3, BV785, Biolegend, #100355, 145-2C11, B303965
anti-CD4, BV650, Biolegend, #100555, RM4-5, B250896
anti-CD8, BV711, BD, #563046, 53-6.7, 0239184
anti-CD69, PECy7, Biolegend, # 104511, H1.2F3, B291440

anti-CD103, PerCP-Cy5.5, BioLegend, #121416, 2E7, B314149
anti-CD44, BV421, Biolegend, #103040, IM7, B306124
anti-CD45, BV605, Biolegend, #103139, 30-F11, B301866
anti-IFNγ, APC, Biolegend, #505810, XMG1.2, B290393a
anti-TNFa, FITC, Biolegend, #506304, MP6-XT22, B271488
anti-IL2, AF700, Biolegend, #503818, JES6-5H4, B335226
anti-IL4, PerCPCy5.5, Biolegend, #504124, 11B11, B301560
anti-CD95, PECy7, BD Biosciences, #557653, Jo2, 0321061
anti-CD19, PerCP-Cy5.5, BioLegend, #115534, 6D5,B288784
anti-CD38, BUV395, BD Biosciences, #740245, 90,1242465
anti-CD44 , APC-Cy7, BioLegend, #103062, IM7, B290267
anti-CD138, BV605, BD Biosciences, #563147, 281-2, 1097493
anti-CD3, A700, BioLegend, #100216, 17A2, B323639
anti-CD4, BV650, BioLegend, #100469,GK1.5, B311210
anti-CXCR5, BV711, BioLegend, #145529, L138D7,B315903
anti-PD1, PECF594, BioLegend, #135228, 29F.1A12, B320108
anti-γδ TCR, A488, BioLegend, #144611, GL3, B343654

Validation

All antibodies used were evaluated by the manufacturers as provided in their websites.
Biolegend:https://www.biolegend.com/en-us/quality/product-development
BD:https://www.biocompare.com/Antibody-Manufacturing/355107-Antibody-Manufacturing-Perspectives-BD-Bioscience/
Thermofisher: https://www.thermofisher.com/us/en/home/life-science/antibodies/invitrogen-antibody-validation.html

## Animals and other organisms

Policy information about studies involving animals; ARRIVE guidelines recommended for reporting animal research

Laboratory animals

C57BL/6, B6129SF2/J, Tlr2-/-, Tlr3-/-, Tlr4-/-, and Tlr5-/- mice were purchased from Jackson Laboratories. Ripk3-/-, Gsdmd-/-, and littermates were gifts from Genentech Inc (Alex Gitlin). Ifnar1-/-, Mda5-/-, Sting-/-, cGas-/-, and Batf3-/- mice were bred in our animal facility at Stanford University. Asc-/- and Nlrp3-/- mice were originally from Vishva M Dixit lab in Genetech, Tlr7-/- mice were originally from S.Akira lab (Osaka University). Asc-/-, Nlrp3-/- and Tlr7-/- mice were then maintained and provided by Jackson Laboratories. Mice were sex-matched and aged between 8 and 14 weeks.

Wild animals

No wild animals were used in this study.

Field-collected samples

No field-collected samples were used in this study.

Ethics oversight

All mice in this study were maintained under specific pathogen-free conditions, 12 light/12 dark cycle, temperatures of ~18-23°C with 40-60% humidity, and handled according to the protocol approved by the Institutional Animal Care and Use Committee (IACUC) of Stanford University.

Note that full information on the approval of the study protocol must also be provided in the manuscript.

## Flow Cytometry

### Plots

Confirm that:

☒ The axis labels state the marker and fluorochrome used (e.g. CD4-FITC).

☒ The axis scales are clearly visible. Include numbers along axes only for bottom left plot of group (a 'group' is an analysis of identical markers).

☒ All plots are contour plots with outliers or pseudocolor plots.

☒ A numerical value for number of cells or percentage (with statistics) is provided.

### Methodology

Sample preparation

1, Flow cytometry analysis of innate cells: Draining iliac lymph nodes from BNT162b2 immunized mice, draining inguinal lymph nodes from YF-17D immunized mice, along with whole lung or spleen, were harvested and digested with 1 mg/mL collagenase type IV (Worthington) for 20 min at 37 °C, followed by smashing with a 100 µm strainer to make a single-cell suspension. Red blood cells from the lung and spleen were lysed before staining.
2, Flow cytometry of GC B, TFH, and plasma cells in lymph nodes: dLNs were harvested and smashed with a 100 µm strainer to make a single-cell suspension followed by staining for viability with Ghost Dye Violet 510 (Tonbo Biosciences) for 5 min on ice in 1x PBS-2mM EDTA.
3, Intracellular cytokine staining assay: Whole Spleen and lung were harvested at 42 days post-prime (21 days post-boost). Briefly, mononuclear populations from the lung were isolated from the interphase of a 70-40% Percoll gradient of single suspension prepared by enzymatic digestion with 1 mg/mL type IV collagenase and DNase I. Single-cell suspensions from the spleen were prepared without digestion. Cells were plated at ~2 x 10^6 cells/well in 96-well U-shaped plates and re-stimulated with S-specific overlapping peptide pools (1 µg/mL of each peptide) in complete RPMI1640 medium for overnight

incubation at 37 °C in the presence of brefeldin-A (10 µg/mL). At day 2, cells were stained with Ghost Dye Violet 510 (Tonbo Biosciences) for 10 min on ice in 1x PBS-2mM EDTA.
4, scRNAseq samples and preparation: Draining iliac lymph nodes from BNT162b2 immunized mice and draining inguinal lymph nodes from YF-17D immunized mice were harvested and digested into single-cell suspensions. One million total cells were set aside on ice. The rest of the cells were incubated with biotinylated CD3, CD19, and NK1.1 Ab on ice for 20 min. Streptavidin-labeled magnetic beads (BD IMag™ Streptavidin Particles Plus-DM) were added and incubated on ice for 30 min. Unbonded cells were collected and CD11b+ myeloid cells, pDCs (CD11clo, CD11b-PDCA-1+), and DCs (CD11c+MHC-II+) were sorted with flow cytometry. Sorted cells were combined with total lymphocytes at a 1:1 ratio and resuspended in cold PBS supplemented with 1% BSA (Miltenyi) and 0.5 U/µL RNase Inhibitor (Sigma Aldrich). Cells were partitioned into Gel Beads-in emulsion (GEMs) using the 10x Chromium 3' V3 chemistry system (10x Genomics).

Instrument

Cells were analyzed with an LSRII.2 or BD FACSymphony analyzer at the Stanford Shared FACS Facility.

Software

BD FACSDiva software version 8.0.1 was used for collecting the flow cytometry data on the LSRII.2 machine.
FlowJo software v.10.0 (Treestar Inc) was used to analyze the flow cytometry data.

Cell population abundance

For scRNAseq samples and preparation: CD11b+ myeloid cells, pDCs (CD11clo, CD11b-PDCA-1+), and DCs (CD11c+MHC-II+) were sorted with flow cytometry after remove CD3, CD19, and NK1.1 with Streptavidin-labeled magnetic beads (BD IMag™ Streptavidin Particles Plus-DM). Sorted cells were combined with total lymphocytes at a 1:1 ratio and resuspended in cold PBS supplemented with 1% BSA (Miltenyi) and 0.5 U/µL RNase Inhibitor (Sigma Aldrich) for scRNAseq analysis.

Gating strategy

Cells were selected based on FSC-A vs. SSC-A, singlets were selected using FSC-A vs. FSC-H. Live CD45+CD3+ T cells were used for analysis of antigen-specific T cells. CD4 and CD8 T cells were selected as CD3+CD8-CD4+ or CD3+ CD8+. Live CD45+CD3 +CD19-CD4+PD1+CXCR5+ T cells were gated as TFH cells, Live CD45+CD3-CD19+CD38-CD95+ cells were gated as GC B cells, Live CD44+CD138+ cells were gated as plasma cells. Gating strategies for innate immune cells, NKT, and γδ T cells are provided in the manuscript.

☒ Tick this box to confirm that a figure exemplifying the gating strategy is provided in the Supplementary Information.